

# The proteasome antechamber maintains substrates in an unfolded state

Amy M. Ruschak<sup>1</sup>, Tomasz L. Religa<sup>1</sup>, Sarah Breuer<sup>2</sup>, Susanne Witt<sup>2</sup> & Lewis E. Kay<sup>1</sup>

Eukaryotes and archaea use a protease called the proteasome that has an integral role in maintaining cellular function through the selective degradation of proteins<sup>1–4</sup>. Proteolysis occurs in a barrel-shaped 20S core particle, which in *Thermoplasma acidophilum* is built from four stacked homoheptameric rings of subunits,  $\alpha$  and  $\beta$ , arranged  $\alpha_7\beta_7\beta_7\alpha_7$  (ref. 5). These rings form three interconnected cavities, including a pair of antechambers (formed by  $\alpha_7\beta_7$ ) through which substrates are passed before degradation and a catalytic chamber ( $\beta_7\beta_7$ ) where the peptide-bond hydrolysis reaction occurs<sup>4,5</sup>. Although it is clear that substrates must be unfolded to enter through narrow, gated passageways (13 Å in diameter) located on the  $\alpha$ -rings<sup>1,6,7</sup>, the structural and dynamical properties of substrates inside the proteasome antechamber remain unclear. Confinement in the antechamber might be expected to promote folding and thus impede proteolysis. Here we investigate the folding, stability and dynamics of three small protein substrates in the antechamber by methyl transverse-relaxation-optimized NMR spectroscopy<sup>8</sup>. We show that these substrates interact actively with the antechamber walls and have drastically altered kinetic and equilibrium properties that maintain them in unstructured states so as to be accessible for hydrolysis.

Each proteasome core particle (Fig. 1a) can accumulate multiple substrates that distribute among all three chambers, supporting a

model whereby the antechambers function as reservoirs for toxic proteins before degradation<sup>9,10</sup>. It is therefore expected that the conformations adopted by substrates within the antechamber are critical in controlling the rate and efficacy of protein hydrolysis. One possibility is that the antechamber might function as an inert chamber that promotes folding<sup>11</sup>. A simple thermodynamic argument predicts that confinement would lead to the relative stabilization of the native state conformation by means of an entropic effect that limits the conformations accessible to the unfolded polypeptide<sup>12</sup>. However, refolding of substrates while they are ‘stored’ is undesirable as many sites would become inaccessible to cleavage.

To address the structural and motional properties of substrate in the proteasome antechamber, we have used transverse-relaxation-optimized NMR spectroscopy to exploit the sensitivity of methyl groups as probes in high-molecular-weight proteins<sup>8,13</sup>. Stable substrate–proteasome complexes have been produced by tethering substrate molecules to the proteasome through a 15 Å heterobifunctional reagent that links the substrate amino terminus to a cysteine located on the surface of the  $\alpha$ -subunit (Fig. 1a and Supplementary Fig. 1), with substrate release occurring only on incubation with reducing agent (Supplementary Fig. 2). As described in Methods, on average each antechamber is populated by approximately one substrate molecule. Three substrates have been chosen, including the engrailed homeodomain from

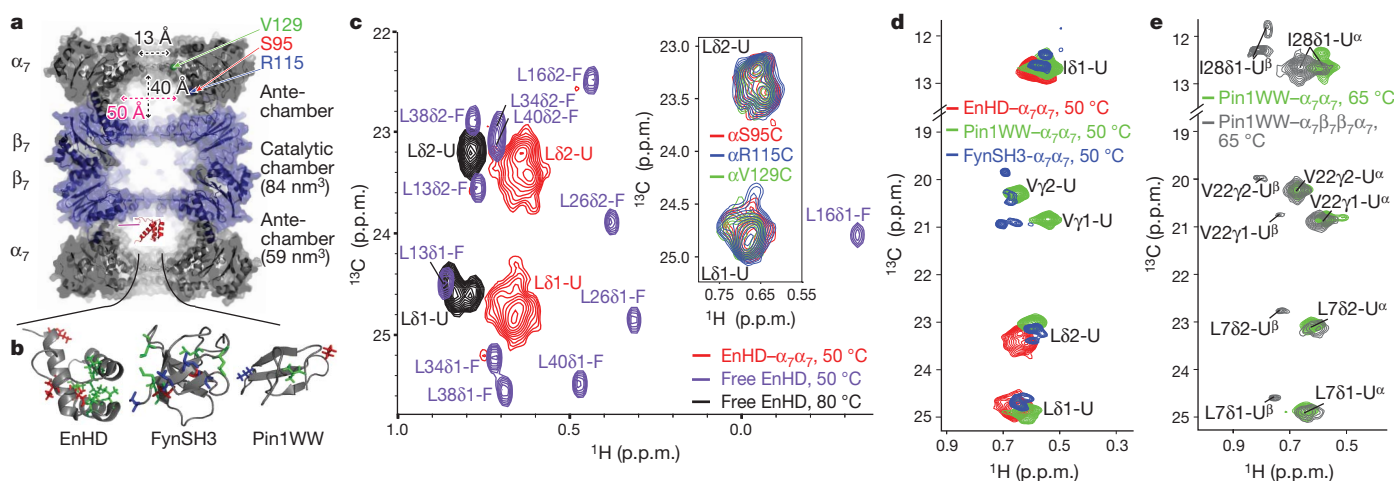


**Figure 1 | Encapsulation of substrates in  $\alpha_7\alpha_7$ .** **a**, Structure of the proteasome from *T. acidophilum*<sup>5</sup>, with red, green and blue spheres designating the locations of Ser 95, Val 129 and Arg 115 in the  $\alpha$ -subunit that have been used for substrate tethering. **b**, Native structures of proteasome substrates EnHD, FynSH3 and Pin1WW. The locations of Ile (red), Leu (green) and Val (blue) probes are shown using a stick representation. **c**, Spectrum of the Leu region of EnHD in  $\alpha_7\alpha_7$  (red) and free in solution (purple), at 50 °C. For reference, the spectrum of the temperature-denatured state of free EnHD at 80 °C is shown (black). Inset, HMQC spectra of EnHD attached to residues 95 (red), 115 (blue) and 129 (green) of the  $\alpha$ -subunit in  $\alpha_7\alpha_7$ , at 50 °C. **d**, Spectra of EnHD (red), Pin1WW

(green) and FynSH3 (blue) encapsulated at Ser 95 of  $\alpha_7\alpha_7$ , at 50 °C. The spectrum of FynSH3 was recorded using different buffer conditions; the best overlay with the Pin1WW and EnHD spectra was achieved by translating the spectrum 0.19 p.p.m. in the  $^1\text{H}$  dimension. **e**,  $^{13}\text{C}, ^1\text{H}$  HMQC spectrum of ILV-methyl-labelled Pin1WW encapsulated in an active-site mutant of  $\alpha_7\beta_7\beta_7\alpha_7$  (grey) and in  $\alpha_7\alpha_7$  (green), at 65 °C. The extra set of peaks for  $^{13}\text{CH}_3$ -Pin1WW in the full proteasome derives from substrate localized to the catalytic chamber (denoted by superscript 'β') as opposed to the antechamber (superscript 'α'). On average, only one Pin1WW is tethered per antechamber. Figures displaying molecular structures were made with PyMOL (<http://www.pymol.org>).

<sup>1</sup>Departments of Molecular Genetics, Biochemistry and Chemistry, The University of Toronto, Toronto, Ontario M5S 1A8, Canada. <sup>2</sup>Department of Structural Biology, Max Planck Institute of Biochemistry, Am Kloppferspitz 18, 82152 Martinsried, Germany.

*Drosophila melanogaster*<sup>14</sup> (EnHD), a FYN Src homology 3 domain from *Gallus gallus*<sup>15</sup> (FynSH3) and the WW domain from *Homo sapiens* PIN1<sup>16</sup> (Pin1WW). These proteins provide examples of different secondary structures and charge states at the pH studied (pH 6.8; Fig. 1b), from  $\alpha$ -helical (EnHD; isoelectric point, pI = 11.7) to predominantly  $\beta$ -sheet (Pin1WW, pI = 11.3; FynSH3, pI = 4.3). Notably, all three proteins are readily degraded upon incubation with the core particle (Supplementary Fig. 3).

Initial studies focused on a two-ring system,  $\alpha_7\alpha_7$ , which spontaneously assembles from wild-type  $\alpha$  monomers in the absence of the  $\beta$ -subunit (ref. 17). We have chosen  $\alpha_7\alpha_7$  as a model for the antechamber ( $\alpha_7\beta_7$ ) for two reasons: first, the  $\alpha$ - and  $\beta$ -subunits are structurally homologous<sup>5</sup> and the amino-acid compositions of surface-exposed side chains in the  $\alpha$ - and  $\beta$ -subunits are very similar; second, the small size of the particle (360 kDa) relative to the full proteasome (670 kDa) leads to significantly better <sup>13</sup>C,<sup>1</sup>H heteronuclear multiple quantum coherence (HMQC) correlation spectra that can be quantified more rigorously<sup>18</sup>. It is worth noting, however, that similar results are obtained when using the full  $\alpha_7\beta_7\beta_7\alpha_7$  construct (see below). To assess the conformation and dynamics of each substrate, ILV-methyl-labelled substrates (corresponding to U-[<sup>2</sup>H] Ile-[ $\delta$ 1<sup>3</sup>CH<sub>3</sub>], Leu,Val-[<sup>13</sup>CH<sub>3</sub>,<sup>12</sup>CD<sub>3</sub>] labelling<sup>13</sup>) were produced and tethered to U-[<sup>2</sup>H]  $\alpha_7\alpha_7$ . At 50 °C, the spectrum of encapsulated EnHD, which is linked to position 95 of the  $\alpha$ -subunit, contains clusters of broad peaks that derive from each methyl type (Fig. 1c, red). Similar to what is observed for the temperature-denatured state of EnHD free in solution at 80 °C (Fig. 1c, black), the spectrum lacks dispersion and <sup>13</sup>C <sup>$\delta$ 1</sup>/<sup>13</sup>C <sup>$\delta$ 2</sup> chemical-shift differences are as expected for an ensemble of unfolded conformers<sup>19</sup>. This picture is very different from the well-resolved correlation map recorded at 50 °C (Fig. 1c, purple) of the folded 7.7-kDa protein. Tethering of EnHD is not responsible for unfolding, as attachment of the linker to its N terminus does not alter its fold or stability, and linking EnHD to a monomeric version of the  $\alpha$ -subunit at the same position (S95C; Supplementary Figs 4 and 5) or on the outside of  $\alpha_7\alpha_7$  (Supplementary Fig. 5) has no effect on the structure of EnHD. Finally, EnHD was conjugated to either of two additional positions in the  $\alpha_7\alpha_7$  chamber:  $\alpha$ R115C and  $\alpha$ V129C (Fig. 1a). The <sup>13</sup>C,<sup>1</sup>H correlation maps of the three distinctly attached domains are essentially identical (Fig. 1c, inset), such that the tether position does not bias the conformational states sampled by EnHD in  $\alpha_7\alpha_7$ . It is expected that most EnHD residues could access the entire space enclosed by  $\alpha_7\alpha_7$  (diameter,  $\sim$ 50 Å; ref. 5), because the root mean

squared end-to-end distance of denatured EnHD is predicted to be  $\sim$ 70.6  $\pm$  1.5 Å (ref. 20), with the linker extending 15 Å.

The <sup>13</sup>C,<sup>1</sup>H HMQC spectra of Pin1WW and FynSH3 encapsulated in  $\alpha_7\alpha_7$  at 50 °C (tethered at position 95) are very similar to that of EnHD, establishing that they too lack well defined, ordered structure under these conditions (Fig. 1d). A similar conclusion is obtained in studies of Pin1WW attached to the  $\alpha$ -subunit (position 95) of an active-site mutant of  $\alpha_7\beta_7\beta_7\alpha_7$ , Pin1WW- $\alpha_7\beta_7\beta_7\alpha_7$  (65 °C). Spectra consist of two sets of peaks (Fig. 1e); one set overlies those of Pin1WW- $\alpha_7\alpha_7$  and the second set, which also derives from an unfolded state, corresponds to substrate localized to the catalytic chamber (Supplementary Fig. 6).

Although only a limited temperature range could be explored in NMR studies of Pin1WW- $\alpha_7\beta_7\beta_7\alpha_7$  because of the size of the complex, a much more extensive NMR investigation was possible for Pin1WW- $\alpha_7\alpha_7$  and FynSH3- $\alpha_7\alpha_7$ , where spectra recorded at 25 °C indicate that both Pin1WW (Fig. 2a) and FynSH3 (Supplementary Fig. 7) become predominantly folded at this temperature. The linewidths of peaks in spectra recorded for FynSH3- $\alpha_7\alpha_7$  are similar to those of the free protein, suggesting that interactions with the cavity are minimal for the folded domain. The spectrum of Pin1WW- $\alpha_7\alpha_7$  at 25 °C contains clusters of peaks (Fig. 2a, magenta) that are located near those of the native, unencapsulated state (Fig. 2a, black). The clustering is not the result of multiple Ile, Leu and Val probes, as this domain contains only one residue of each. Rather, Pin1WW seems to exist in several distinct 'native-like' states in slow exchange that may reflect interactions with the cavity wall (see below). Finally, unlike both Pin1WW and FynSH3, EnHD- $\alpha_7\alpha_7$  remains unfolded over the complete temperature range examined, which extends as low as 10 °C (Supplementary Fig. 7), despite the fact that in the free state EnHD has a melting temperature of 64 °C (Supplementary Fig. 4).

We used Pin1WW to evaluate how the kinetics and thermodynamics of folding change on encapsulation. To compare the folding properties of encapsulated and free Pin1WW domains, we acquired HMQC spectra over the temperature ranges 5–50 °C (Pin1WW- $\alpha_7\alpha_7$ , tethered at  $\alpha$ S95C), 5–80 °C (free Pin1WW) and 40–65 °C (stabilized mutant of Pin1WW<sup>21</sup>, tethered to  $\alpha$ S95C of an active-site mutant of the full proteasome, Pin1WW2- $\alpha_7\beta_7\beta_7\alpha_7$ ). Pin1WW is an ultrafast-folding protein (microsecond timescale<sup>22</sup>). Consistent with this, the folding/unfolding of the free Pin1WW domain was found to be fast on the NMR chemical-shift timescale, with peak positions given by

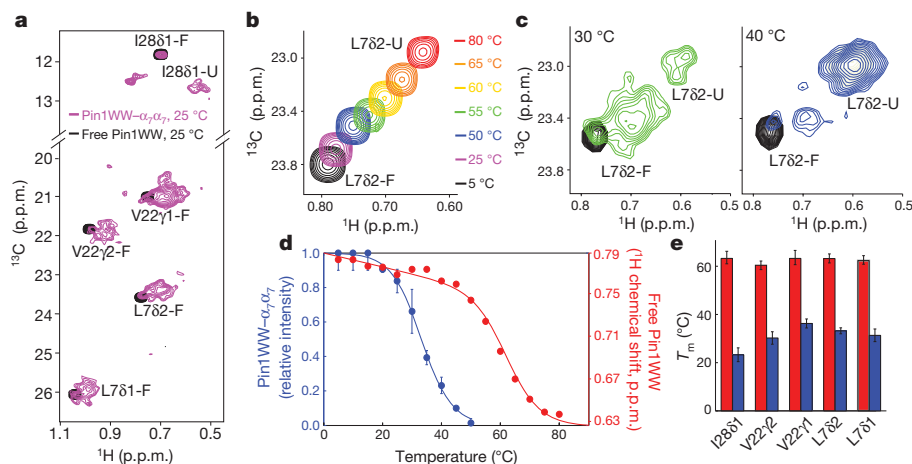


**Figure 2 | Folding of proteasome substrates in  $\alpha_7\alpha_7$ .** **a**, Spectrum of ILV-methyl-labelled Pin1WW in  $\alpha_7\alpha_7$  at 25 °C (magenta). Free Pin1WW is shown in black as a reference. **b**, **c**, Spectral regions showing the temperature dependence of the L782 methyl peak for Pin1WW free in solution (**b**) and tethered to  $\alpha_7\alpha_7$  (**c**). **d**, Representative melting curves for L782 of free (red) and  $\alpha_7\alpha_7$ -encapsulated (blue) Pin1WW, derived using either chemical shifts (free Pin1WW) or the relative peak intensities of unfolded and folded states

(encapsulated Pin1WW). Fits to standard equations for two-state melting<sup>30</sup> are shown (solid lines). **e**,  $T_m$  values derived from fits for each of the methyl groups for free (red) and encapsulated (blue) Pin1WW. For Pin1WW- $\alpha_7\alpha_7$ , error bars are based on measurements of three separate samples. For free Pin1WW, error bars in chemical shifts, based on triplicate measurements ( $<$ 0.3 p.p.b. for <sup>13</sup>C and  $<$ 0.1 p.p.b. for <sup>1</sup>H), are too small to be visible relative to the size of the marker.

population-weighted averages of those for the unfolded and folded states (Fig. 2b). By contrast, separate sets of peaks are observed for the folded and unfolded states of Pin1WW- $\alpha_7\alpha_7$  (Fig. 2c) and Pin1WW2- $\alpha_7\beta_7\beta_7\alpha_7$ ; for Pin1WW2- $\alpha_7\beta_7\beta_7\alpha_7$  these derive from substrate localized to the antechamber (Supplementary Fig. 8). Peak intensities for folded and unfolded states change in intensity as a function of temperature (Fig. 2c), indicating that on encapsulation folding/unfolding is slow on the chemical-shift timescale. An upper bound on  $k_f + k_u$  of  $\sim 5 \text{ s}^{-1}$  at 32.5 °C, where  $k_f$  and  $k_u$  are respectively the folding and unfolding rates, was estimated on the basis of the absence of cross-peaks in magnetization exchange spectra of Pin1WW- $\alpha_7\alpha_7$ . This bound is at least four orders of magnitude less than the values of  $k_f$  and  $k_u$ ,  $\sim 10^4$ – $10^5 \text{ s}^{-1}$ , obtained for the free protein<sup>16</sup>.

The stability of Pin1WW- $\alpha_7\alpha_7$  is also drastically reduced. We generated melting profiles from the temperature dependence of peak intensities and positions in HMQC spectra, providing estimates of melting temperature,  $T_m$ , for Pin1WW- $\alpha_7\alpha_7$  and, respectively, free Pin1WW, as shown in Fig. 2d. The Pin1WW domain free in solution folds by means of a two-state mechanism, with Ile, Leu and Val probes reporting a  $T_m$  value of  $62.4 \pm 1.3$  °C. By contrast, the  $T_m$  value for Pin1WW- $\alpha_7\alpha_7$  ranges from  $23.2 \pm 2.8$  to  $36.2 \pm 1.8$  °C depending on the methyl probe (Fig. 2e). The non-uniformity of  $T_m$  values indicates that Pin1WW- $\alpha_7\alpha_7$  does not fold/unfold by means of a two-state mechanism, by contrast to free Pin1WW<sup>23</sup>. Similarly, at 65 °C there is a range in the relative intensities of folded versus unfolded peaks in spectra of Pin1WW2- $\alpha_7\beta_7\beta_7\alpha_7$ , corresponding to substrate being 18–32% folded inside the proteasome antechamber under conditions where it is 85% folded in solution, an extent of destabilization that is very nearly the same as for encapsulation in  $\alpha_7\alpha_7$  at 65 °C (Supplementary Table 1).

NMR spin relaxation experiments have been performed to establish whether Pin1WW- $\alpha_7\alpha_7$  interacts with the walls of the cavity, which would lead to significant increases in the overall tumbling time,  $\tau_C$ , of the encapsulated protein. Values of  $S_{\text{axis}}^2 \tau_C$  were measured<sup>24</sup> at 50 °C for Pin1WW- $\alpha_7\alpha_7$ , where  $S_{\text{axis}}^2$  is a squared order parameter quantifying the amplitude of motion of the methyl-axis bond vector (0 (mobile)  $\leq S_{\text{axis}}^2 \leq 1$  (rigid)).  $S_{\text{axis}}^2 \tau_C$  values for Pin1WW- $\alpha_7\alpha_7$  range between 30 and 50 ns (Fig. 3a, blue); by contrast  $S_{\text{axis}}^2 \tau_C \approx 1$  ns is obtained for residues of free Pin1WW at 50 °C (Fig. 3a, red). The larger  $S_{\text{axis}}^2 \tau_C$  values for Pin1WW- $\alpha_7\alpha_7$  cannot be explained by increases in viscosity inside the cavity because <sup>1</sup>H transverse-relaxation rates of the stabilized mutant Pin1WW2, which is largely folded inside  $\alpha_7\alpha_7$  at 50 °C, were identical for encapsulated and free states at this temperature (Supplementary Fig. 9). Rather, because such values are similar to those obtained for ILV methyls of  $\alpha_7\alpha_7$  ( $S_{\text{axis}}^2 \tau_C \approx 70$  ns at 50 °C; Fig. 3a, grey), they must reflect the fact that the wild-type Pin1WW domain interacts strongly with the cavity walls. Moreover, assuming that the encapsulated Pin1WW domain is rigidly bound to the walls of  $\alpha_7\alpha_7$  such that it tumbles with the rotational correlation time of the particle,  $\tau_C = 120$  ns at 50 °C (ref. 18),  $S_{\text{axis}}^2$  values of between 0.27 and 0.41 are calculated from measured  $S_{\text{axis}}^2 \tau_C$  times, consistent with the level of ordering expected for an unfolded substrate<sup>25</sup>.

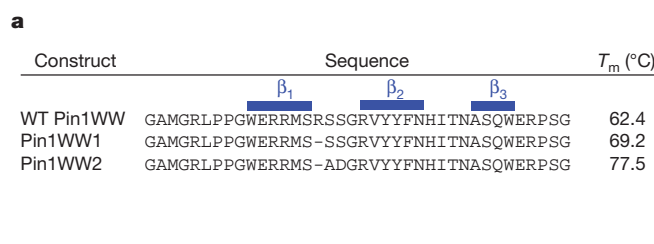


**Figure 4 | Substrate stability and proteolysis rates are anticorrelated.** **a**, Primary sequence of the WW constructs used, with  $T_m$  values (free form) as indicated<sup>21</sup>. The locations of  $\beta$ -strands are highlighted. **b**, Correlation between the  $T_m$  value of the free substrate and the extent of substrate proteolysis.

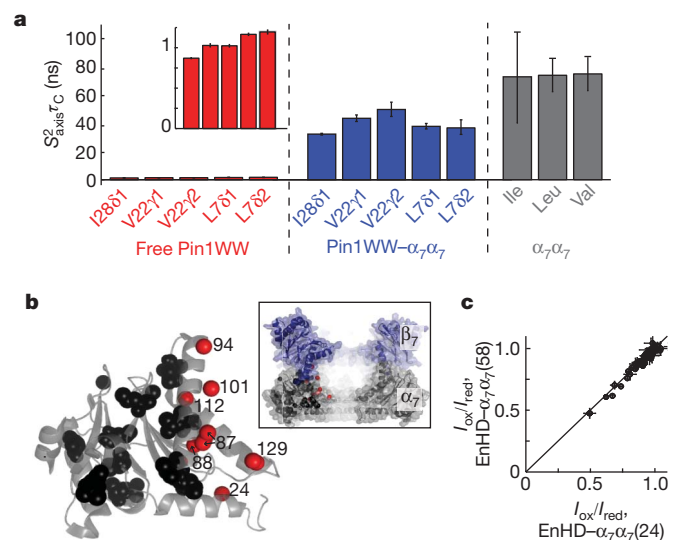


**Figure 3 | Interactions between unfolded substrates and the  $\alpha$ -ring.** **a**,  $S_{\text{axis}}^2 \tau_C$  values for Ile, Leu and Val probes in free Pin1WW (red), Pin1WW- $\alpha_7\alpha_7$  (blue) and  $\alpha_7\alpha_7$  (grey). Errors for Pin1WW are estimated on the basis of a Monte Carlo error analysis. In the case of  $\alpha_7\alpha_7$ , the average  $S_{\text{axis}}^2 \tau_C$  values for the 65% of methyl groups that are intermediate in the distribution for each residue type are indicated along with error bars corresponding to 1 s.d. **b**, Positions of  $\alpha$ -subunit methyl groups whose peaks show >10% (red) or <10% (black) intensity change upon addition of nitroxide-labelled EnHD (attached to residue 24) in  $\alpha_7\alpha_7$ . The orientation of the single  $\alpha$ -particle in the context of  $\alpha_7\beta_7$  is as indicated in the inset. **c**, Comparison of intensity ratios with and without conjugation of nitroxide spin label to residues 24 and 58 of EnHD in  $\alpha_7\alpha_7$ . All substrates are tethered to position 95 of the  $\alpha$ -subunit.  $I_{\text{ox}}$  and  $I_{\text{red}}$  are the  $\alpha_7\alpha_7$  peak intensities with and without TEMPO labelling, respectively. Errors are based on propagated uncertainties in measurement of  $I_{\text{ox}}$  and  $I_{\text{red}}$  values.

Having established that there are definite interactions between substrate and cavity, we measured how encapsulation of substrates (tethered to position 95) alters the chemical shifts and relaxation properties of  $\alpha$ -subunit ILV methyl groups in either  $\alpha_7\alpha_7$  or  $\alpha_7\beta_7\beta_7\alpha_7$ . Only very small changes were observed (Supplementary Fig. 10), suggesting that encapsulation has little effect on the conformation or dynamics of the  $\alpha$ -subunit. Nitroxide spin labels increase relaxation rates of methyl probes in a distance-dependent manner, resulting in an attenuation of peak intensities in NMR spectra<sup>26,27</sup>. Attachment of such a label at positions 24 and 58 of EnHD in an EnHD- $\alpha_7\alpha_7$  complex produced nearly identical decreases in intensities (paramagnetic relaxation enhancements<sup>26,27</sup>) of ILV methyl probes of  $\alpha_7\alpha_7$ , affecting methyl groups located within 20 Å of the inside surface of the cavity (Fig. 3b, c). These results establish that EnHD is located exclusively inside  $\alpha_7\alpha_7$  and does not sample regions outside the chamber that would require substrate to exit through the  $\alpha$ -annuli. Moreover, they imply that different residues of EnHD do not have unique, position-dependent interactions with the surface of the cavity, suggesting that the domain is

best described in terms of an ensemble of dynamic, interconverting, unstructured conformations. Patterns of paramagnetic relaxation enhancements from analogous experiments conducted with spin-labelled Pin1WW encapsulated in either  $\alpha_7\alpha_7$  or  $\alpha_7\beta_7\beta_7\alpha_7$  were quantitatively very similar to those measured for EnHD (Supplementary Fig. 11).

To determine the importance of maintaining substrate in an unfolded state for proteolysis, we measured the extent to which three Pin1WW domains of varying stabilities ( $T_m$ ; Fig. 4a) are degraded by the proteasome over a fixed time. These Pin1WW domains have different relative populations of folded and unfolded states in the antechamber (wild-type Pin1WW is unfolded in  $\alpha_7\alpha_7$  at 50 °C (Fig. 1d), whereas Pin1WW2 is largely folded (Supplementary Fig. 9)). Each of the three Pin1WW domains was tethered to position S95C of the  $\alpha$ -subunit in an  $\alpha_7\beta_7\beta_7\alpha_7$  construct (wild-type  $\beta$ -subunit) that is inhibited by calpain inhibitor 1. After tether release and the subsequent removal of inhibitor at 4 °C, the substrate–proteasome complex was heated to 50 °C for 5 or 15 min (Fig. 4b and Supplementary Fig. 12), and the extent of degradation that occurred during incubation at 50 °C was determined by reverse-phase high-performance liquid chromatography. The inverse correlation between substrate stability and the extent of proteolysis (Fig. 4b) implies that unfolded states are processed and proteolyzed more efficiently than folded states<sup>8</sup>.

We have shown that interactions with the proteasome antechamber significantly shift both the stability and the folding/unfolding rates of substrate so as to disfavour refolding, in a manner that seems to be unrelated to substrate secondary structure, topology and surface charge. In this context, the proteasome antechamber actively primes substrates for subsequent degradation.

## METHODS SUMMARY

**Production of encapsulated samples.** Proteins were overexpressed using <sup>13</sup>C-labelled precursors and growth media as described in Methods. We produced  $\alpha_7\alpha_7$  samples as outlined in Methods, with one surface-exposed cysteine per chamber on average. Heterobifunctional linking reagent, LC-SPDP (Pierce), was attached to the N terminus of the substrate and after purification the linker substrate was incubated with  $\alpha_7\alpha_7$  overnight to generate an encapsulated sample, as verified by SDS–polyacrylamide gel electrophoresis (Supplementary Fig. 1). In the case of  $\alpha_7\beta_7\beta_7\alpha_7$  encapsulation samples, each  $\alpha$ -subunit contained the S95C mutation, and each  $\beta$ -subunit contained a T1A (inactivating) mutation<sup>28</sup> and included a four-residue polyglycine prosequence. Substrate was added, at a substrate/ $\alpha$ -subunit molar ratio of 1:7, to yield on average one substrate per antechamber. Final protein concentrations for NMR were 70–430  $\mu$ M in  $\alpha_7\alpha_7$  complex with 70–430  $\mu$ M in substrate, and 35–110  $\mu$ M in  $\alpha_7\beta_7\beta_7\alpha_7$  with 70–220  $\mu$ M in substrate. All NMR samples were dissolved in 100% D<sub>2</sub>O buffer, 1 mM EDTA, 0.03% Na<sub>3</sub> and 25 mM potassium phosphate, pH 6.8, 50 mM NaCl (Pin1WW, EnHD) or 20 mM Tris, pH 8.0 (FynSH3).

Methyl transverse-relaxation-optimized (HMQC) spectra<sup>8</sup> were recorded at 5–50 °C using 500-, 600- and 800-MHz Varian Inova spectrometers equipped with cryogenically cooled (600 MHz) or room-temperature (500 and 800 MHz) pulsed-field-gradient triple-resonance probes. All data for  $\alpha_7\alpha_7$  or  $\alpha_7\beta_7\beta_7\alpha_7$  recorded at temperatures >50 °C were acquired at 800 MHz. Chemical shifts were referenced against 2,2-dimethyl-2-silapentane-5-sulphonic acid. Assignments for  $\alpha$ -subunit ILV methyl groups in  $\alpha_7\alpha_7$  and  $\alpha_7\beta_7\beta_7\alpha_7$  were obtained from published values<sup>18</sup>. All data were processed with the NMRPipe suite of programs<sup>29</sup> and analysed using either NMRPipe/NMRDraw or FUDA (<http://pound.med.utoronto.ca/software.html>).

**Full Methods** and any associated references are available in the online version of the paper at [www.nature.com/nature](http://www.nature.com/nature).

Received 3 May; accepted 23 August 2010.

1. Förster, A. & Hill, C. P. Proteasome degradation: enter the substrate. *Trends Cell Biol.* **13**, 550–553 (2003).
2. Coux, O., Tanaka, K. & Goldberg, A. L. Structure and functions of the 20S and 26S proteasomes. *Annu. Rev. Biochem.* **65**, 801–847 (1996).
3. Baumeister, W., Walz, J., Zühl, F. & Seemüller, E. The proteasome: paradigm of a self-compartmentalizing protease. *Cell* **92**, 367–380 (1998).
4. Marques, A. J., Palaninurugan, R., Matias, A. C., Ramos, P. C. & Dohmen, R. J. Catalytic mechanism and assembly of the proteasome. *Chem. Rev.* **109**, 1509–1536 (2009).

5. Löwe, J. *et al.* Crystal structure of the 20S proteasome from the archaeon T. acidophilum at 3.4 Å resolution. *Science* **268**, 533–539 (1995).
6. Liu, C. W., Corboy, M. J., DeMartino, G. N. & Thomas, P. J. Endoproteolytic activity of the proteasome. *Science* **299**, 408–411 (2003).
7. Cheng, Y. Toward an atomic model of the 26S proteasome. *Curr. Opin. Struct. Biol.* **19**, 203–208 (2009).
8. Tugarinov, V., Hwang, P. M., Ollerenshaw, J. E. & Kay, L. E. Cross-correlated relaxation enhanced <sup>1</sup>H–<sup>13</sup>C NMR spectroscopy of methyl groups in very high molecular weight proteins and protein complexes. *J. Am. Chem. Soc.* **125**, 10420–10428 (2003).
9. Sharon, M. *et al.* 20S proteasomes have the potential to keep substrates in store for continual degradation. *J. Biol. Chem.* **281**, 9569–9575 (2006).
10. Hutschenreiter, S., Tinazli, A., Model, K. & Tampé, R. Two-substrate association with the 20S proteasome at single-molecule level. *EMBO J.* **23**, 2488–2497 (2004).
11. Ellis, R. J. Protein folding: importance of the Anfinsen cage. *Curr. Biol.* **13**, R881–R883 (2003).
12. Zhou, H. X. Protein folding in confined and crowded environments. *Arch. Biochem. Biophys.* **469**, 76–82 (2008).
13. Ruschak, A. M. & Kay, L. E. Methyl groups as probes of supra-molecular structure, dynamics and function. *J. Biomol. NMR* **46**, 75–87 (2010).
14. Mayor, U. *et al.* The complete folding pathway of a protein from nanoseconds to microseconds. *Nature* **421**, 863–867 (2003).
15. Neudecker, P. *et al.* Identification of a collapsed intermediate with non-native long-range interactions on the folding pathway of a pair of Fyn SH3 domain mutants by NMR relaxation dispersion spectroscopy. *J. Mol. Biol.* **363**, 958–976 (2006).
16. Jager, M. *et al.* Understanding the mechanism of beta-sheet folding from a chemical and biological perspective. *Biopolymers* **90**, 751–758 (2008).
17. Zwickl, P., Kleinz, J. & Baumeister, W. Critical elements in proteasome assembly. *Nature Struct. Biol.* **1**, 765–770 (1994).
18. Sprangers, R. & Kay, L. E. Quantitative dynamics and binding studies of the 20S proteasome by NMR. *Nature* **445**, 618–622 (2007).
19. Wishart, D. S., Bigam, C. G., Holm, A., Hodges, R. S. & Sykes, B. D. <sup>1</sup>H, <sup>13</sup>C and <sup>15</sup>N random coil NMR chemical shifts of the common amino acids. I. Investigations of nearest-neighbor effects. *J. Biomol. NMR* **5**, 67–81 (1995).
20. Fitzkee, N. C. & Rose, G. D. Reassessing random-coil statistics in unfolded proteins. *Proc. Natl Acad. Sci. USA* **101**, 12497–12502 (2004).
21. Jäger, M. *et al.* Structure-function-folding relationship in a WW domain. *Proc. Natl Acad. Sci. USA* **103**, 10648–10653 (2006).
22. Kubelka, J., Hofrichter, J. & Eaton, W. A. The protein folding ‘speed limit’. *Curr. Opin. Struct. Biol.* **14**, 76–88 (2004).
23. Jäger, M., Nguyen, H., Crane, J. C., Kelly, J. W. & Gruebele, M. The folding mechanism of a beta-sheet: the WW domain. *J. Mol. Biol.* **311**, 373–393 (2001).
24. Tugarinov, V., Sprangers, R. & Kay, L. E. Probing side-chain dynamics in the proteasome by relaxation violated coherence transfer NMR spectroscopy. *J. Am. Chem. Soc.* **129**, 1743–1750 (2007).
25. Choy, W. Y., Shortle, D. & Kay, L. E. Side chain dynamics in unfolded protein states: an NMR based <sup>2</sup>H spin relaxation study of  $\Delta$ 131 $\Delta$ . *J. Am. Chem. Soc.* **125**, 1748–1758 (2003).
26. Battiste, J. L. & Wagner, G. Utilization of site-directed spin labeling and high-resolution heteronuclear nuclear magnetic resonance for global fold determination of large proteins with limited nuclear Overhauser effect data. *Biochemistry* **39**, 5355–5365 (2000).
27. Clore, G. M., Tang, C. & Iwahara, J. Elucidating transient macromolecular interactions using paramagnetic relaxation enhancement. *Curr. Opin. Struct. Biol.* **17**, 603–616 (2007).
28. Kisselev, A. F., Songyang, Z. & Goldberg, A. L. Why does threonine, and not serine, function as the active site nucleophile in proteasomes? *J. Biol. Chem.* **275**, 14831–14837 (2000).
29. Delaglio, F. *et al.* NMRPipe: a multidimensional spectral processing system based on UNIX pipes. *J. Biomol. NMR* **6**, 277–293 (1995).
30. Fersht, A. *Structure and Mechanism in Protein Science* (Freeman, 1999).

**Supplementary Information** is linked to the online version of the paper at [www.nature.com/nature](http://www.nature.com/nature).

**Acknowledgements** The authors would like to thank J. Forman-Kay for providing laboratory space and for discussions, R. Muhandiram for NMR support, H. Lin for help designing protein purification protocols, X. Li and A. Shimmer for assistance with the plate reader, and W. Baumeister for discussions. T.L.R. acknowledges The European Molecular Biology Organization (ALTF 827-2006) and The Canadian Institutes of Health Research (CIHR) for postdoctoral fellowships. L.E.K. holds a Canada Research Chair in Biochemistry. This work was supported by grants from the CIHR and the Natural Sciences and Engineering Research Council of Canada.

**Author Contributions** A.M.R. made samples. T.L.R. helped make plasmids for protein expression and trained A.M.R. to express and purify proteins. A.M.R. and L.E.K. designed experiments, recorded and analysed NMR data, and wrote the manuscript. S.B. and S.W. were involved in preliminary experimental design, and S.W. and T.L.R. commented on the manuscript.

**Author Information** Reprints and permissions information is available at [www.nature.com/reprints](http://www.nature.com/reprints). The authors declare no competing financial interests. Readers are welcome to comment on the online version of this article at [www.nature.com/nature](http://www.nature.com/nature). Correspondence and requests for materials should be addressed to L.E.K. ([kay@pound.med.utoronto.ca](mailto:kay@pound.med.utoronto.ca)).

## METHODS

**Protein expression.** All proteins were produced by expression in *Escherichia coli* BL21(DE3) codon plus cells, using minimal media with [ $^{12}\text{C}$ ,  $^2\text{H}$ ] glucose as the sole carbon source in 99%  $\text{D}_2\text{O}$  or using lysogeny broth for  $^1\text{H}$  (unlabelled) protein. In the case of ILV-methyl-labelled protein samples, the labelling was U- $^{13}\text{C}$  Ile- $[\delta 1^{13}\text{CCH}_3]$ , Leu,Val- $^{13}\text{CCH}_3$ ,  $^{12}\text{CD}_3$ . Such samples were generated by addition of  $60\text{ mg l}^{-1}$  of 2-keto-3,3- $\text{D}_2$ -4- $^{13}\text{C}$ -butyrate (Ile) and  $80\text{ mg l}^{-1}$  2-keto-3-methyl- $\text{D}_3$ -3- $\text{D}_1$ -4- $^{13}\text{C}$ -butyrate (Leu,Val) to the media 1 h before induction, as previously described<sup>13,31</sup>.

**Mutagenesis.** Mutations for all proteasome and substrate constructs were introduced by site-directed mutagenesis using the Stratagene Quikchange kit. Because lysine residues are known to cross-react with the heterobifunctional crosslinking reagent used to link the substrate to the wall of the proteasome (Supplementary Fig. 1 legend), all lysine residues in substrates have been mutated to arginine except for Lys 52 of EnHD, which was instead mutated to alanine as this had been previously reported to stabilize EnHD<sup>14,32</sup>. The stabilized Pin1WW mutant used in some of the studies reported in the text (referred to as Pin1WW2 in what follows:  $T_m = 77.5^\circ\text{C}$ ,  $k_f, k_u = 10^5\text{--}10^6\text{ s}^{-1}$ ; ref. 21) has an altered loop composition between the first two  $\beta$ -strands (the triplet Arg 17-Ser 18-Ser 19 was changed to the amino-acid pair Ala-Asp; variant two in fig. 1 of ref. 21). In addition to constructing substrate-linked  $\alpha_7\alpha_7$  and  $\alpha_7\beta_7\alpha_7$ , we also generated substrate-linked  $\alpha$ -subunit. The following mutations were used to stabilize the  $\alpha$  monomer: deletion from residues 2 to 34, R57A, R86A, R130A (as was used previously to assign the  $\alpha$  monomer in  $\alpha_7\alpha_7$  and  $\alpha_7\beta_7\alpha_7$ <sup>18</sup>), S95C and C151S. All protein constructs were verified using ESI ( $\alpha$ -subunit,  $\beta$ -subunit, FynSH3 and EnHD) or MALDI (Pin1WW) mass spectrometry.

**Protein purification and substrate encapsulation.** The  $\alpha$  and  $\beta$  subunits (referred to in what follows as  $\alpha$  and  $\beta$ , respectively) were expressed as fusion proteins with a TEV-cleavable His tag in cells grown at  $37^\circ\text{C}$  ( $\alpha$ ) or with a NusA-His tag in cells grown at  $16^\circ\text{C}$  ( $\beta$ ). Cells expressing  $\alpha$  and  $\beta$  were lysed by sonication in 50 mM phosphate buffer (pH 8.0), 100 mM NaCl, 10 mM imidazole, 1 mM DTT (buffer A) with the addition of an EDTA-free protease inhibitor cocktail tablet (Roche), and lysozyme. After centrifugation at 39,000g for 45 min, the supernatant was loaded onto a HiTrap Ni-NTA column (GE Healthcare), washed extensively with buffer A and eluted using buffer A plus 250 mM imidazole. Final purification of  $\alpha$  was achieved by size-exclusion chromatography (Superdex 200, 100 mM NaCl, 50 mM phosphate (pH 7.5) (GF buffer)), whereas for  $\beta$  purification involved dialysis in 20 mM Tris (pH 8.0), followed by anion exchange chromatography on a monoQ column (20 mM Tris (pH 8.0)), with elution using a NaCl gradient from 0 to 1 M.

We prepared  $\alpha_7\alpha_7$ , consisting of a 1:14 mixture of  $\alpha$ -cysteine mutant and wild-type  $\alpha$ , by mixing the two  $\alpha$  constructs together (with His tags still attached) at the desired molar ratio (1:14) and then performing buffer exchange into 6 M Gdn HCl, 50 mM phosphate (pH 7.5), 100 mM NaCl and 5 mM DTT, so that the total  $\alpha$  concentration was 50  $\mu\text{M}$ . After heating at  $50^\circ\text{C}$  for 1 h, the solution was allowed to cool to room temperature ( $\sim 23^\circ\text{C}$ ) and then diluted 20-fold by volume into GF buffer plus 2 mM DTT at  $0.1\text{ ml min}^{-1}$  with rapid stirring. The protein was concentrated using a HiTrap Ni-NTA column and subsequently purified by size-exclusion chromatography to remove improperly refolded  $\alpha$ .

The full proteasome ( $\alpha_7\beta_7\alpha_7$ ) was assembled by mixing  $\alpha$  (100–150  $\mu\text{M}$  in GF buffer) and  $\beta$  (30–60  $\mu\text{M}$  in 20 mM Tris (pH 8.0) and  $\sim 200\text{ mM}$  NaCl) at  $37^\circ\text{C}$  overnight, and typically assembly was driven to completion by using a slight molar excess of  $\alpha$  over  $\beta$ . Unassembled components were removed from the intact proteasomes using a Superdex 200 column.

All substrates were expressed as fusion proteins with TEV-cleavable His tags. Cells expressing EnHD were grown at  $37^\circ\text{C}$  and those expressing FynSH3, Pin1WW and Pin1WW2 were grown at  $25^\circ\text{C}$ . Cell lysis was achieved by sonicating resuspended cells in 6 M Gdn HCl, 50 mM phosphate (pH 8.0), 100 mM NaCl and 10 mM imidazole. The protein of interest (EnHD, FynSH3, Pin1WW or Pin1WW2) was bound to a Ni-NTA HiTrap column and eluted using an analogously prepared buffer with 400 mM imidazole. Substrates were refolded by dialysis into 50 mM phosphate (pH 7.0) and 50 mM NaCl (EnHD, Pin1WW and Pin1WW2) or 50 mM phosphate (pH 8.0) and 100 mM NaCl (FynSH3). EnHD and Pin1WW were purified using a HiTrap SP column (GE Healthcare) and eluted with a NaCl gradient from 50 to 1,000 mM; Pin1WW2 and FynSH3 were purified using a Superdex 75 column. His tags were cleaved and unconjugated His tag and TEV were removed using Ni-NTA affinity chromatography.

Heterobifunctional linking reagent, LC-SPDP (Pierce), was attached to the N terminus of the substrate by incubating linker in 10-fold molar excess (50  $\text{mg ml}^{-1}$  DMSO stock) with substrate (20  $\mu\text{M}$ ) for 2 h (50 mM phosphate and 100 mM NaCl (pH 7.5)). Unreacted linker was removed by buffer exchange using a concentrator ( $M_w$  3,000 Da cut-off). The linker substrate was then incubated with  $\alpha_7\alpha_7$  overnight ( $50^\circ\text{C}$  in 50 mM phosphate (pH 7.5) and 100 mM NaCl for Pin1WW;

$50^\circ\text{C}$  in 20 mM Tris (tris(hydroxymethyl)aminomethane; pH 8.0) for EnHD;  $25^\circ\text{C}$  in 50 mM phosphate (pH 7.5) and 100 mM NaCl for FynSH3) with a 1.5 molar excess of substrate over  $\alpha$ -cysteine concentration. Encapsulation was verified by SDS-polyacrylamide gel electrophoresis (SDS-PAGE; Supplementary Fig. 1); unlinked substrate was removed by gel filtration (Superdex 200).

Encapsulation of substrate into the full proteasome ( $\alpha_7\beta_7\alpha_7$ ) was achieved by two different strategies. (1) Pin1WW was conjugated to  $\alpha\text{S95C}$  (1 Pin1WW  $\alpha$  to 7  $\alpha\text{S95C}$ ) and then assembled with  $\beta$  (containing the  $\beta\text{T1A}$  mutation, rendering the proteasome inactive<sup>28</sup>, and a GGGG prosequence) to make the full proteasome. (2) Proteasomes were first assembled and then incubated with linker substrate ( $50^\circ\text{C}$ ). Samples of U- $^{13}\text{C}$  Ile- $[\delta 1^{13}\text{CCH}_3]$ , Leu,Val- $^{13}\text{CCH}_3$ ,  $^{12}\text{CD}_3$ -Pin1WW (WT Pin1WW) linked to  $\alpha_7\beta_7\alpha_7$  prepared by the two methods produced identical  $^{13}\text{C}$ ,  $^1\text{H}$  correlation spectra. However, the stability of the Pin1WW2 was high enough that the first method resulted in greater encapsulation efficiencies (that is, insufficient amounts of Pin1WW2 could be unfolded to facilitate entry into the full proteasome using method 2).

**Preparation of spin-labelled samples.** Cysteine substrate mutants were stored with 10 mM DTT in either SP elution buffer (50 mM phosphate (pH 7.0) and typically several hundred millimolar in NaCl that was necessary for elution of substrate from the HiTrap SP column; see above) or GF elution buffer until immediately before labelling, whereupon the buffer was exchanged for 100 mM NaCl and 50 mM phosphate (pH 7.0). Labelling was achieved by overnight incubation at  $25^\circ\text{C}$  with tenfold molar excess of TEMPO (*N*-(1-oxyl-2,2,6,6-tetramethyl-4-piperidinyl)maleimide, Toronto Research Chemicals), which was added from a freshly prepared 200 mM DMSO stock. The reaction was quenched by buffer exchange using a concentrator with a  $M_w$  3,000 Da cut-off. Labelling was shown to occur at a single position by mass spectrometry. TEMPO was used as it makes an irreversible linkage to the cysteine sulphhydryl, avoiding any possible complications due to disulphide exchange with the LC-SPDP linker that might occur using other types of spin label, such as MTSL.

Spectra of Pin1WW encapsulated in  $\alpha_7\beta_7\alpha_7$  showed two sets of unfolded peaks (Fig. 1e). To assign these sets of peaks (Supplementary Fig. 6), samples were prepared with the spin label attached either in the antechamber (position 95) or in the catalytic chamber (position G-1C, that is, on the tetra-G prosequence). Spin-labelling of the antechamber was achieved as follows. The encapsulation sample ( $\alpha\text{S95C}$ ,  $\beta\text{T1A}$   $\alpha_7\beta_7\alpha_7$  with the GGGG prosequence and Pin1WW conjugated through the linker at one S95C site per antechamber) was incubated overnight with tenfold molar excess of MTSL ((1-oxyl-2,2,5,5-tetramethyl- $\Delta 3$ -pyrroline-3-methyl) methanethiosulfonate, Toronto Research Chemicals) in GF buffer (pH 7.5) at  $25^\circ\text{C}$ . As with TEMPO, MTSL was added from a 200 mM DMSO stock. The reaction was quenched by buffer exchange into NMR buffer. These conditions did not result in labelling at undesired locations, as determined by mass spectrometry. Furthermore, even though both MTSL- $\alpha\text{S95C}$  and  $\alpha$ -substrate are linked by disulphides, the addition of a spin label did not effect conjugation of the substrate, as evidenced by SDS-PAGE. TEMPO was not used to spin-label the proteasome (but was used for spin-labelling of substrate; see above) because it was observed to react at undesired locations in  $\alpha$ . In the case where a spin label was added to the catalytic chamber at  $\beta\text{G-1C}$ , purified  $\beta$  (immediately after Ni-NTA affinity chromatography) in its NusA-His-tagged form was incubated overnight with tenfold molar excess of MTSL in 20 mM Tris (pH 7.5) at  $5^\circ\text{C}$ . The reaction was quenched by buffer exchange into 20 mM Tris (pH 8.0), after which the His tag was cleaved using TEV in the absence of DTT and purified using a monoQ column with subsequent assembly into proteasomes.

**Measurement of paramagnetic relaxation enhancement values.** We measured paramagnetic relaxation enhancement values, providing qualitative information on the interactions between substrate and antechamber, by comparing peak intensities in  $^{13}\text{C}$ ,  $^1\text{H}$  correlation maps recorded on samples of U- $^{13}\text{C}$  Ile- $[\delta 1^{13}\text{CCH}_3]$ , Leu,Val- $^{13}\text{CCH}_3$ ,  $^{12}\text{CD}_3$ - $\alpha_7\alpha_7$  encapsulated with either TEMPO-labelled  $^1\text{H}$  substrate ( $I_{\text{ox}}$ ) or  $^1\text{H}$  substrate ( $I_{\text{red}}$ ). The addition of substrate (no TEMPO label) has a very small effect on peak positions in  $^{13}\text{C}$ ,  $^1\text{H}$  HMQC spectra<sup>18</sup> and  $^1\text{H}$   $R_2$  relaxation rates, relative to  $\alpha_7\alpha_7$  without substrate. By contrast, changes in peak intensities were noted for encapsulation of  $^1\text{H}$  Pin1WW in  $\alpha_7\beta_7\alpha_7$ . Thus, comparing peak intensities recorded on a pair of samples (with and without TEMPO) that could potentially have (slightly) different levels of encapsulation will introduce errors in paramagnetic relaxation enhancement values. Therefore,  $I_{\text{red}}$  was measured by reducing the nitroxide spin label of the encapsulation sample by reaction with 200 mM ascorbate for 2 h (50 mM phosphate (pH 6.8) and 50 mM NaCl at  $25^\circ\text{C}$ ).

**Measurement of  $R_2$  rates.** Relaxation rates of the slowly relaxing  $^1\text{H}$  single-quantum methyl transitions were measured using the pulse scheme of ref. 33 and processed using the NMRPipe suite of programs<sup>29</sup>. A set of two-dimensional  $^{13}\text{C}$ ,  $^1\text{H}$  data sets were recorded where a variable delay,  $T$  (for the evolution of  $^1\text{H}$  transverse magnetization), was set to 0.7, 2.5, 5, 8, 11, 14, 17 and 22.5 ms (U- $^{13}\text{C}$ )

Ile- $[\delta^{13}\text{C}_3]$ , Leu,Val- $[\text{}^{13}\text{C}_3, \text{}^{12}\text{CD}_3]$  substrates encapsulated in U- $[\text{}^2\text{H}]$ - $\alpha_7\alpha_7$  or U- $[\text{}^2\text{H}]$  Ile- $[\delta^{13}\text{C}_3]$ , Leu,Val- $[\text{}^{13}\text{C}_3, \text{}^{12}\text{CD}_3]$ - $\alpha_7\alpha_7$ , no substrates). For free Pin1WW2, delays were set to 7.5, 20, 40, 60, 80, 100 and 120 ms.  $R_2$  rates were extracted from exponential fits of peak intensity,  $I$ , versus relaxation delay, using the relation  $I = I_0 \exp(-R_2 T)$ .

**Measurement of  $S_{\text{axis}}^2 \tau_C$  values.**  $S_{\text{axis}}^2 \tau_C$  values were measured and analysed as described in ref. 24 using an approach that quantifies the time dependencies of sums ( $I_b$ ) and differences ( $I_a$ ) of magnetization derived from methyl  $^1\text{H}$  single-quantum transitions. For Pin1WW encapsulated in  $\alpha_7\alpha_7$ ,  $I_a$  and  $I_b$  were measured at 50 °C with T values of 1, 2, 4, 6, 9, 10, 12, 14, 16 and 18 ms, and for the free Pin1WW domain they were measured at 5 °C and T = 10, 20, 30, 40 50, 60, 70, 80, 100, 150, 200, 250 and 300 ms. The profiles  $I_a/I_b$  were fitted to

$$\frac{I_a}{I_b} = \frac{-0.5\eta \tanh(\sqrt{\eta^2 + \delta^2} T)}{\sqrt{\eta^2 + \delta^2} - \delta \tanh(\sqrt{\eta^2 + \delta^2} T)}$$

where

$$\eta \approx \frac{9}{10} [P_2(\cos(\theta_{\text{axis,HH}}))]^2 \frac{S_{\text{axis}}^2 \gamma_{\text{H}}^4 \hbar^2 \tau_C}{r_{\text{HH}}^6}$$

Here  $\tau_C$  is the tumbling time of the particle, which is assumed to be isotropically rotating;  $S_{\text{axis}}^2$  is the square of an order parameter quantifying the amplitudes of

motion of the methyl three-fold symmetry axis;  $\delta$  is a fitting parameter that takes into account the  $^1\text{H}$  density around the methyl group in question;  $\gamma_{\text{H}}$  is the gyromagnetic ratio of a proton spin;  $r_{\text{HH}}$  is the distance between pairs of methyl protons (1.813 Å);  $P_2(x) = (3x^2 - 1)/2$ ; and  $\theta_{\text{axis,HH}}$  is the angle (90°) between the methyl three-fold axis and the vector that connects a pair of methyl  $^1\text{H}$  nuclei. The values of  $S_{\text{axis}}^2 \tau_C$  listed in Fig. 3a were measured for free Pin1WW at 5 °C and subsequently extrapolated to 50 °C using the known change in  $\text{D}_2\text{O}$  viscosity between the two temperatures<sup>34</sup>, assuming that  $S_{\text{axis}}^2$  values are invariant with temperature. We used this procedure rather than direct measurements at the higher temperature because values of  $S_{\text{axis}}^2$  calculated using  $^1\text{H}$ -based relaxation methods are known to be in error when molecules are outside the J(0) limit<sup>24</sup>. The values of  $S_{\text{axis}}^2 \tau_C$  for  $\alpha_7\alpha_7$  were obtained from previously published work<sup>24</sup>.

- Sprangers, R., Velyvis, A. & Kay, L. E. Solution NMR of supramolecular complexes: providing new insights into function. *Nature Methods* **4**, 697–703 (2007).
- Stollar, E. J. *et al.* Crystal structures of engrailed homeodomain mutants: implications for stability and dynamics. *J. Biol. Chem.* **278**, 43699–43708 (2003).
- Tugarinov, V. & Kay, L. E. Relaxation rates of degenerate  $^1\text{H}$  transitions in methyl groups of proteins as reporters of side-chain dynamics. *J. Am. Chem. Soc.* **128**, 7299–7308 (2006).
- Matsunaga, N. & Nagashima, A. Transport properties of liquid and gaseous  $\text{D}_2\text{O}$  over a wide range of temperature and pressure. *J. Phys. Chem.* **6**, 1133–1166 (1977).

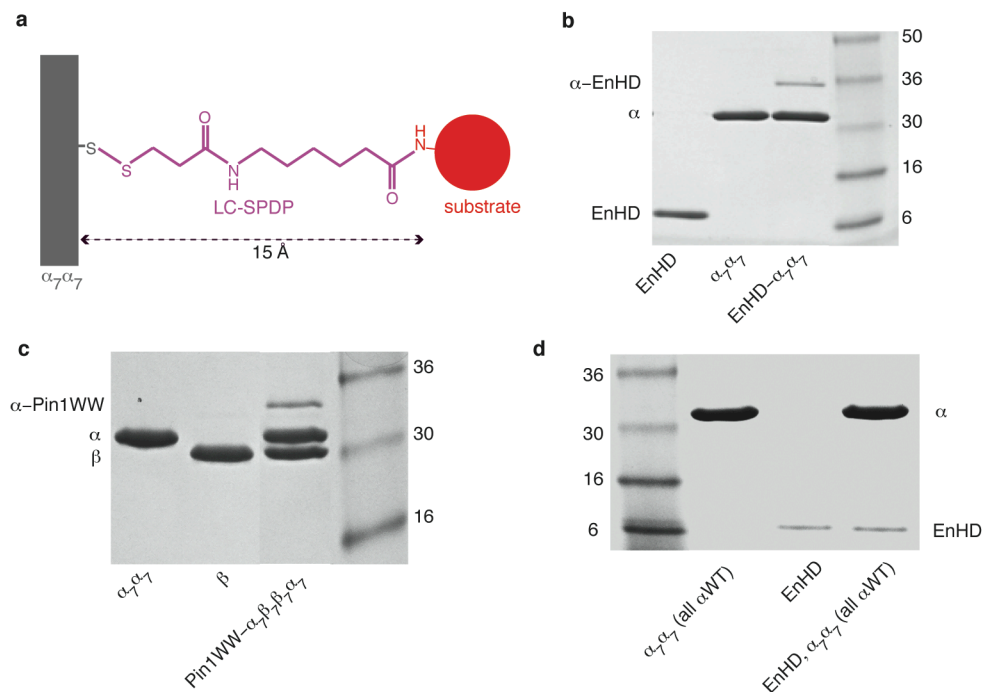


**Figure S1 | Encapsulation of EnHD, Pin1WW and FynSH3 into  $\alpha_7\alpha_7$  or  $\alpha_7\beta_7\beta_7\alpha_7$ .**

**a**, A heterobifunctional cross-linker (LC-SPDP, Pierce) was used to conjugate the N-terminus of the substrate to a cysteine introduced by mutation in  $\alpha$  (S95, R115, or V129).  $\alpha$ -rings were made as a mixture of  $\alpha$ WT and  $\alpha$ -cysteine mutant so that, on average, 1 cysteine mutant (and ultimately 1 substrate molecule) is introduced per chamber. Substrate encapsulation proceeds first by reacting substrate with LC-SPDP, followed by linking to  $\alpha$  by incubation with  $\alpha_7\alpha_7$  or  $\alpha_7\beta_7\beta_7\alpha_7$  under conditions where the substrate is at least 10% unfolded and  $\alpha_7\alpha_7$  /  $\alpha_7\beta_7\beta_7\alpha_7$  is stable (50°C, 100 mM NaCl, 50 mM phosphate, pH 7.5). After overnight incubation of the substrate and  $\alpha_7\alpha_7$  /  $\alpha_7\beta_7\beta_7\alpha_7$  (1.5 substrate – 1  $\alpha_7\alpha_7$  /  $\alpha_7\beta_7\beta_7\alpha_7$ , molar ratios) close to 100% encapsulation efficiencies were observed. Excess substrate was removed by size exclusion chromatography. The conjugation reaction was monitored by SDS PAGE, where a single reaction product was detected, corresponding to the combined masses of  $\alpha$ S95C (~26.1 kDa) and substrate

(EnHD ~7.7 kDa, Pin1WW ~4.4 kDa). Representative gels are shown for encapsulation of EnHD in  $\alpha_7\alpha_7$  (**b**) and Pin1WW in  $\alpha_7\beta_7\beta_7\alpha_7$  (**c**). For specific conjugation between substrate and the linker, the substrate cannot contain lysine sidechains as the linker will react with any primary amine. Therefore substrate lysines were mutated to arginine (in all but one case); this did not compromise the structure or stability of the substrates (data not shown). **d**, The native cysteine of  $\alpha$  at position 151 does not get labeled with substrate. EnHD was incubated with  $\alpha_7\alpha_7$  composed entirely of  $\alpha$ WT under the conditions used in **b** (final lane of the gel in **d**). In this case no cross-linked product ( $\alpha$ -EnHD) was detected (see last lane of gel and note the absence of a peak corresponding to  $\alpha$ -EnHD, compare with EnHD- $\alpha_7\alpha_7$  lane of gel in **b**). Furthermore the intensity of the band corresponding to free EnHD is consistent with the entire amount of EnHD in the reaction. For reference free EnHD was also loaded on the gel in the quantity present in the EnHD,  $\alpha$ WT reaction (3<sup>rd</sup> lane). Therefore the native cysteine of  $\alpha$ WT must be buried in the core of the protein and inaccessible to reaction with the LC-SPDP. Only the cysteines introduced via mutation at positions 95, 115, and 129 are accessible for reaction.

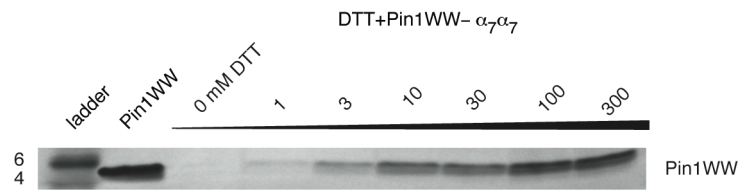


**Figure S2 | Release of the Pin1WW- $\alpha_7\alpha_7$  linker.**

The linker between the substrate and  $\alpha$  contains a disulfide bond which can be released upon addition of reducing agent. To release the substrate linked to  $\alpha_7\alpha_7$ , DTT (1-300 mM) was incubated with Pin1WW- $\alpha_7\alpha_7$  (300  $\mu$ M of the  $\alpha$ -subunit) in 100 mM NaCl, 50 mM phosphate, pH 7.5, for 20 hrs at 25°C. Note,  $\alpha_7\alpha_7$  was composed of a mixture of  $\alpha$ WT and  $\alpha$ S95C to give on average 1  $\alpha$ S95C per  $\alpha_7\alpha_7$  so that 1 substrate molecule is encapsulated per chamber (on average). After incubation the reaction products were separated using a 100 kDa concentrator; Pin1WW- $\alpha_7\alpha_7$  is retained by the membrane, while the released Pin1WW flows through. The flow-through was subsequently analyzed by SDS PAGE. For reference, free Pin1WW was also run (2<sup>nd</sup> lane from left). Increasing amounts of Pin1WW were obtained with increasing amounts of added DTT.

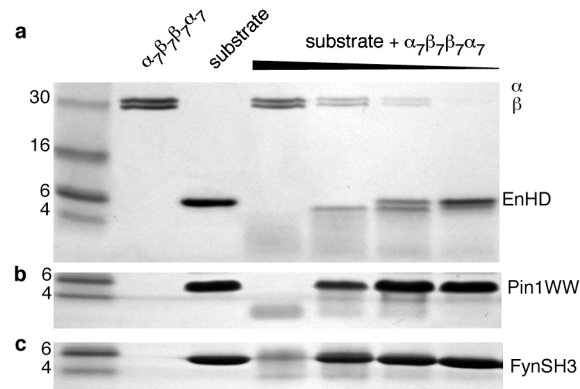


**Figure S3 | EnHD, Pin1WW and FynSH3 are substrates of the WT *T. acidophilum* proteasome.**

500  $\mu$ M EnHD, Pin1WW, or FynSH3 was incubated with a range of proteasome concentrations (790, 260, 88, and 29 nM in complex) for 16 hrs at 50°C (50 mM NaCl, 25 mM phosphate, pH 6.8). Reactions were quenched by denaturation whereby SDS gel loading buffer was added (2% w/v SDS, 4% v/v glycerol, 40 mM Tris pH 6.8, 0.01% bromophenolblue final concentrations) followed by sample heating (90°C, 10 min). The extent of substrate degradation was assessed by SDS PAGE (Tris-glycine gels with a 4-20% acrylamide gradient), as shown for EnHD (a), Pin1WW (b), and FynSH3 (c). Gel lanes (left to right): molecular weight markers, 790 nM proteasome (no substrate), 500  $\mu$ M substrate (no proteasome), and 500  $\mu$ M substrate + proteasome with decreasing concentrations of proteasome (concentrations listed above).

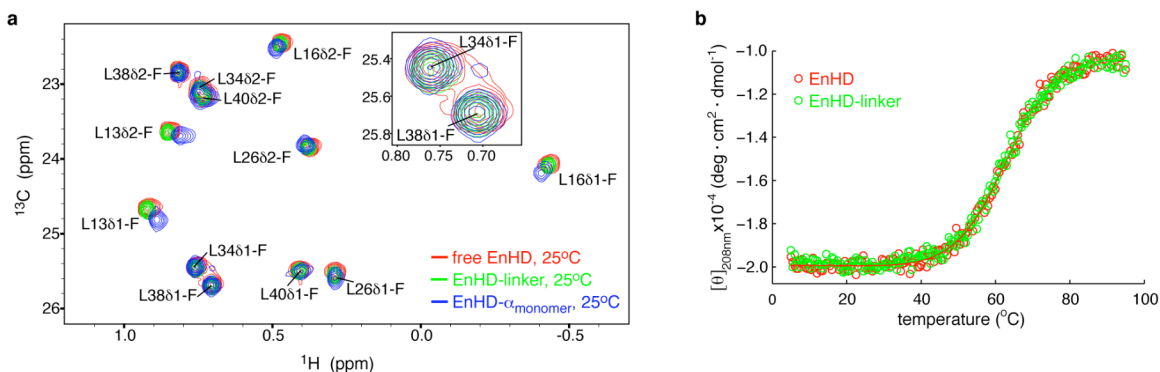


**Figure S4 | The heterobifunctional cross-linker (LC-SPDP) is not responsible for destabilization of EnHD in  $\alpha_7\alpha_7$ .**

**a**, Spectra of the Leu region of free EnHD (red), EnHD-linker (green) and EnHD conjugated to a monomeric version of  $\alpha$  (blue) at 25°C. The spectra of free EnHD and EnHD-linker are indistinguishable, with only very small chemical shift changes in the spectrum of EnHD- $\alpha_{\text{monomer}}$  relative to free EnHD and EnHD-linker. It is clear that EnHD- $\alpha_{\text{monomer}}$  remains folded (peaks labeled as F) in the context of the  $\alpha$  monomer. Inset shows an expanded region emphasizing that L34 $\delta$ 1, L38 $\delta$ 1 peak positions are superimposable for the three EnHD constructs examined. **b**, Thermal denaturation of EnHD and EnHD-linker as measured by far-ultraviolet CD at 208 nm. Raw data are shown as points with lines indicating fits to the standard equation for two-state unfolding<sup>1</sup>. Melting curves for EnHD and EnHD-linker are indistinguishable, establishing that the linker does not alter the stability of EnHD.

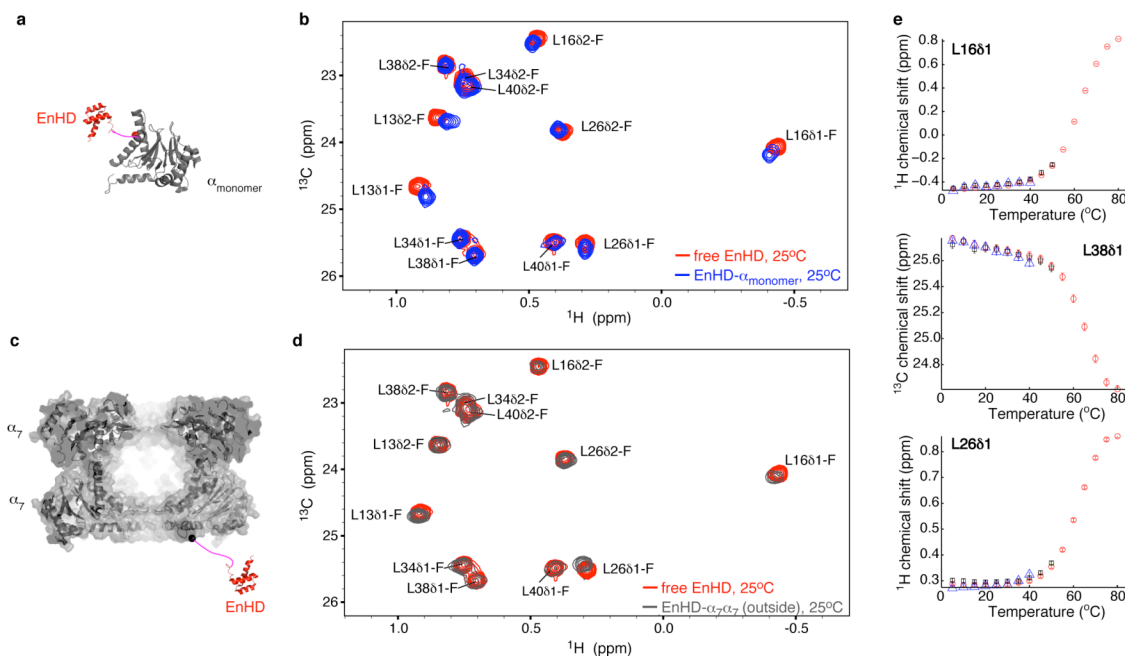


**Figure S5 | EnHD is folded when it is attached to either a monomeric version of  $\alpha$  or to the outside of  $\alpha_7\alpha_7$ .**

**a**, The N-terminus of ILV- $^{13}\text{CH}_3$  EnHD (red) was linked via the heterobifunctional crosslinking reagent, LC-SPDP (magenta), to a cysteine in a monomeric version of  $\alpha$  ( $\alpha_{\text{monomer}}$ , grey), introduced by mutation ( $\alpha$  at position 95 (red sphere)). **b**, Leu region of  $^{13}\text{C}$ ,  $^1\text{H}$  correlation maps of free EnHD (red) and EnHD- $\alpha_{\text{monomer}}$  (blue), 25°C, showing that EnHD remains folded (peaks labeled as F) in the context of  $\alpha_{\text{monomer}}$ , with very small chemical shift changes in the spectrum of EnHD- $\alpha_{\text{monomer}}$  relative to free EnHD. **c**, LC-SPDP (magenta) was used to link the N-terminus of ILV- $^{13}\text{CH}_3$  EnHD (red) to the outside of  $\alpha_7\alpha_7$  (grey) at a cysteine introduced by mutation at position 20 (black sphere),  $\alpha\text{R20C}$ . Note,  $\alpha$ -rings were made as a mixture of  $\alpha\text{WT}$  and  $\alpha\text{R20C}$  so that, on average, there is 1 cysteine (1 site of encapsulation) per  $\alpha$ -ring. **d**, Leu region of  $^{13}\text{C}$ ,  $^1\text{H}$  correlation maps of free EnHD (red) and EnHD- $\alpha_7\alpha_7$  (outside, grey), as described in **c**, establishing

that EnHD is folded when it is linked to the outside of  $\alpha_7\alpha_7$ . This is in contrast to when it is conjugated to a position on the inside of  $\alpha_7\alpha_7$  (Figure 1c), where EnHD is unfolded at all temperatures  $\geq 10^\circ\text{C}$  (see Figure S6c). **e**, Temperature dependence of the  $^{13}\text{C}$  or  $^1\text{H}$  chemical shifts of 3 EnHD peaks for free EnHD (red circles), EnHD- $\alpha_{\text{monomer}}$  (blue triangles), and EnHD- $\alpha_7\alpha_7$  (outside) (grey squares). EnHD folding is in the fast exchange regime so the chemical shifts are a population-weighted average of those for the folded and unfolded states. Therefore, the temperature dependence of  $^{13}\text{C}$  or  $^1\text{H}$  chemical shifts can be used to monitor EnHD folding (see main text). Spectra of EnHD- $\alpha_{\text{monomer}}$  and EnHD- $\alpha_7\alpha_7$  (outside) were recorded from 5-40°C and 5-50°C, respectively, reflecting the temperature ranges over which the constructs remained soluble/stable. Clearly the folding behavior of EnHD in the context of these  $\alpha$  constructs is very similar to free EnHD over the measured temperature range.

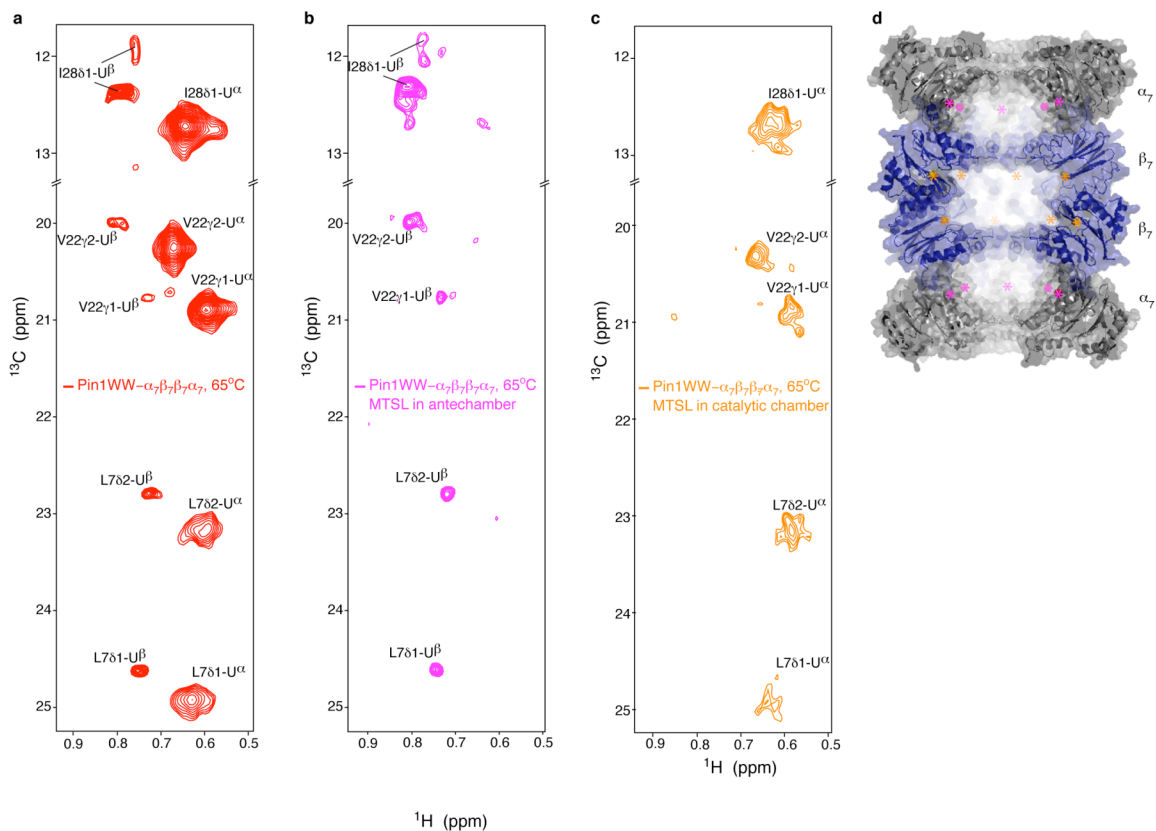


**Figure S6 | Pin1WW is localized to both ante- and catalytic chambers in  $\alpha_7\beta_7\beta_7\alpha_7$ .**

**a**, Spectrum of ILV-methyl labeled Pin1WW in  $\alpha_7\beta_7\beta_7\alpha_7$  at 65°C, where Pin1WW is tethered at residue 95 of  $\alpha$  in the antechamber, with on average 1 Pin1WW domain per antechamber (see Methods). Note that in these  $\alpha_7\beta_7\beta_7\alpha_7$  samples all  $\alpha$  subunits contain the S95C mutation. **b**, Addition of MTSL to the antechamber (at position 95) allows the assignment of sets of peaks in (a) to either the Pin1WW domain in the antechamber (denoted by  $\alpha$ ) or catalytic chamber (denoted by  $\beta$ ). Note that in any antechamber 1 of 7 of component  $\alpha$  subunits is linked with Pin1WW at position 95 (on average) so that the 6 remaining positions are conjugated to MTSL. Addition of MTSL did not disrupt the Pin1WW linkage (data not shown). The peaks that are absent relative to the spectrum in (a) arise from Pin1WW in the antechamber. **c**, Addition of MTSL to G-1C of the pro-sequence in the catalytic chamber (that is inactivated via a T1A mutation) results in

conjugation of spin-label to all 14  $\beta$  subunits in each  $\alpha_7\beta_7\beta_7\alpha_7$  particle and the elimination of peaks arising from Pin1WW localized in the catalytic chamber. **d**, Positions of the spin label in the context of the  $\alpha_7\beta_7\beta_7\alpha_7$  structure. Magenta and orange stars indicate the locations at which the MTSL was attached in  $\alpha$  and  $\beta$  as used for spectra in **(b)** and **(c)**, respectively. The  $\alpha$  and  $\beta$ -rings are colored grey and blue as in Figure 1a of the main text.

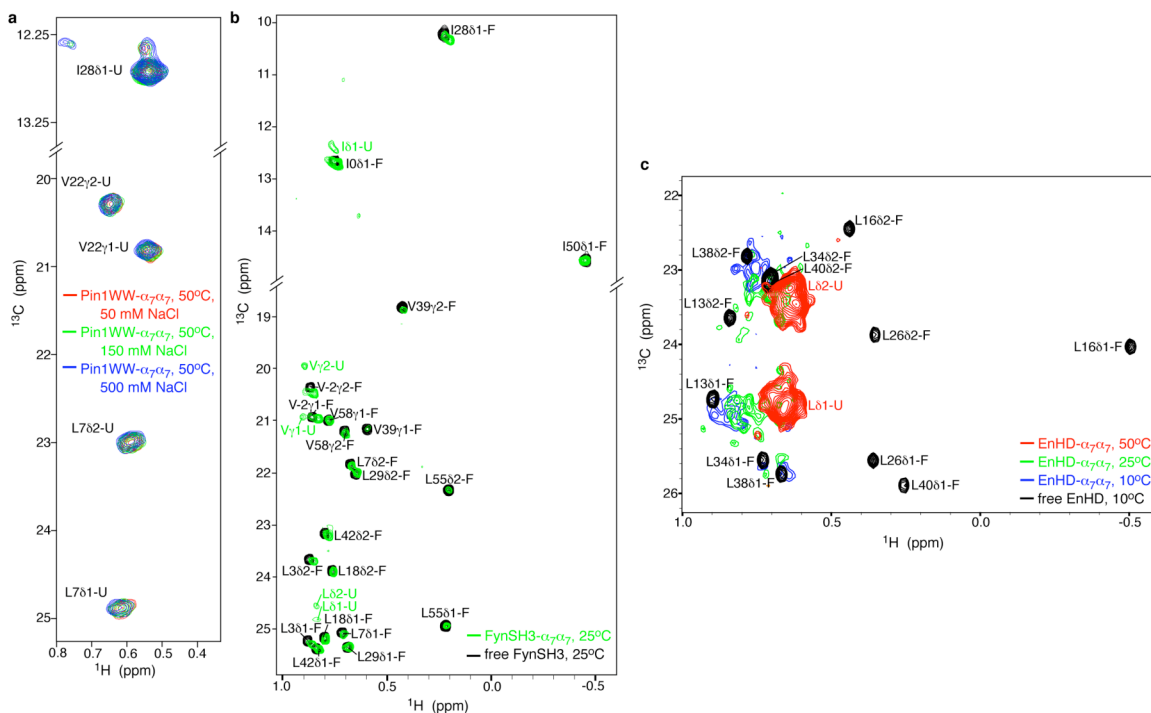


**Figure S7 | Salt and temperature dependence of substrate folding in  $\alpha_7\alpha_7$ .**

**a**,  $^{13}\text{C}, ^1\text{H}$  HMQC spectra of ILV-methyl labeled Pin1WW in  $\alpha_7\alpha_7$ , 50°C, as a function of NaCl concentration (50 mM, red; 150 mM, green; 500 mM, blue). Spectra are independent of [NaCl] from 50 mM to 500 mM, 50°C, indicating that changes in electrostatics upon encapsulation are not primarily responsible for unfolding.

**b**, Spectra of ILV-methyl labeled FynSH3 in  $\alpha_7\alpha_7$  (green) and free in solution (black) at 25°C. Under these conditions FynSH3- $\alpha_7\alpha_7$  is predominantly folded and the peaks of the folded state (labeled as F) overlay well with those for the free form. Weak intensity peaks corresponding to the unfolded state of FynSH3 are also detected in the spectrum of FynSH3- $\alpha_7\alpha_7$  (labeled as U).

**c**, Spectra of the Leu region of ILV-methyl labeled EnHD encapsulated in  $\alpha_7\alpha_7$  at 50°C (red), 25°C (green) and 10°C (blue). For reference the spectrum of free EnHD, 10°C, is shown (black). At 10°C and 25°C peak clusters from EnHD- $\alpha_7\alpha_7$ , derived from the unfolded state, are observed (that shift with temperature)

while only two weak peaks are positioned close to those for free EnHD, indicating that EnHD- $\alpha_7\alpha_7$  is predominately unfolded at these temperatures, in contrast to Pin1WW- $\alpha_7\alpha_7$  and FynSH3- $\alpha_7\alpha_7$ . All substrates were linked to position 95 of the  $\alpha$ -subunit (1 substrate per chamber).

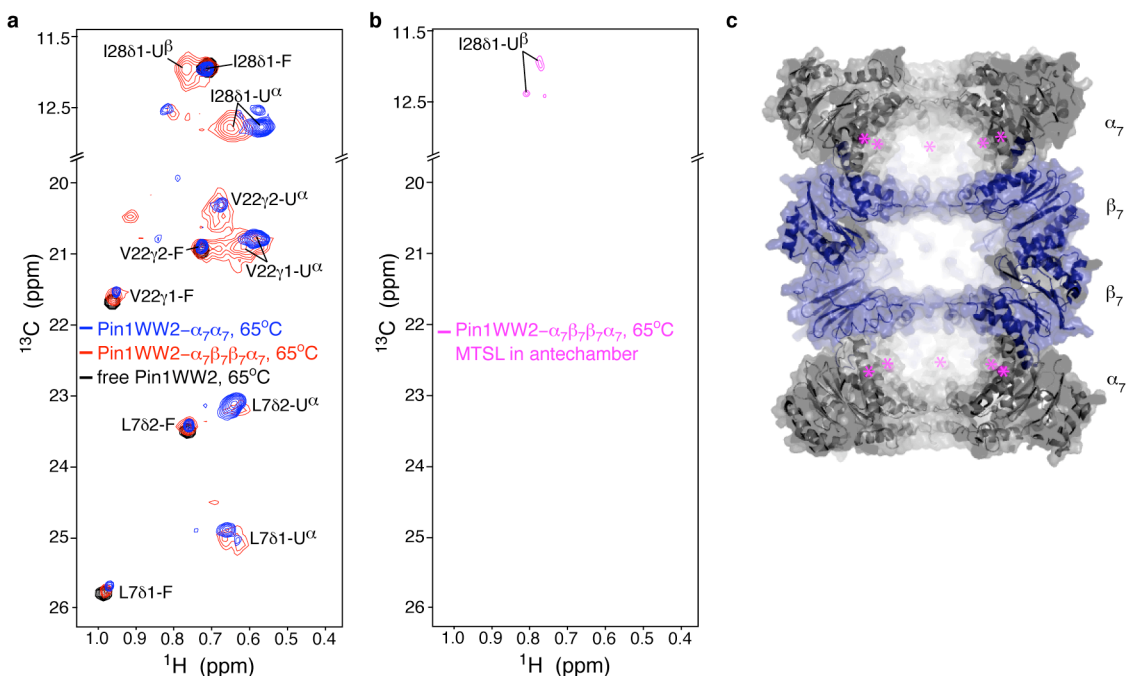


**Figure S8 | The folded and unfolded states of Pin1WW2 reside in the antechamber of  $\alpha_7\beta_7\beta_7\alpha_7$ .**

**a**,  $^{13}\text{C}$ ,  $^1\text{H}$  correlation spectrum of ILV  $^{13}\text{CH}_3$ -Pin1WW2 conjugated at position  $\alpha_95$  in  $\alpha_7\beta_7\beta_7\alpha_7$  at 65°C (red). Peaks corresponding to folded Pin1WW2 are analogous to free Pin1WW2 at 65°C (black), whereas peaks corresponding to the unfolded state are analogous to those observed in  $\alpha_7\alpha_7$  (blue). (Pin1WW2 = Pin1WW from human Pin1 with Arg17-Ser18-Ser19 of the WT protein replaced by the two amino acid sequence Ala-Asp that stabilizes the domain, see Fig. S12a). **b**, Addition of MTSL to the antechamber (at position 95), as in Figure S6, allows assignment of sets of peaks in (a) of Pin1WW2 to the antechamber (denoted by  $\alpha$ ). The absence of all peaks corresponding to the Pin1WW2 folded and unfolded states, as reported by the 5 labeled methyl groups, shows that these states are associated with encapsulation in the antechamber. However, two peaks in the Ile region of the spectrum remain. These peaks derive from the Pin1WW2 in the catalytic chamber (denoted by  $\beta$ ) as they have the same chemical shifts

as Pin1<sup>WW</sup> (WT) in the catalytic chamber of  $\alpha_7\beta_7\beta_7\alpha_7$  at 65°C (Figure S6). **c**, Positions of the spin label are indicated with magenta stars in the context of the  $\alpha_7\beta_7\beta_7\alpha_7$  structure.

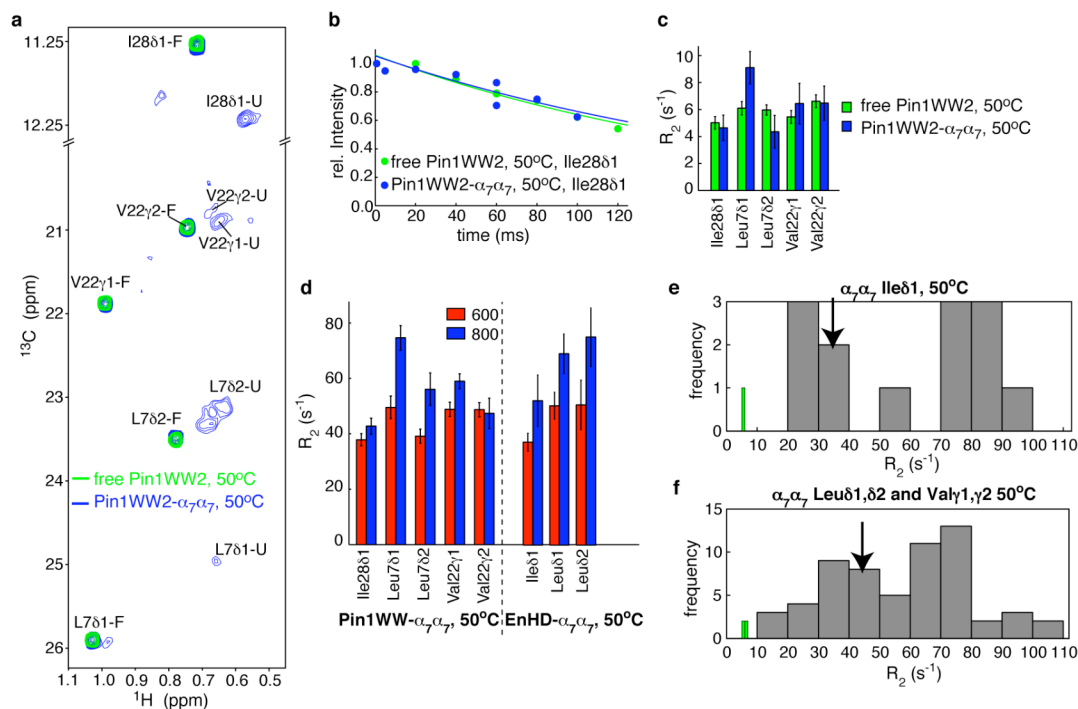


**Figure S9 | Pin1WW2 is predominately folded when encapsulated in  $\alpha_7\alpha_7$  at 50°C and in the folded state does not interact with the cavity walls.**

**a**,  $^{13}\text{C}$ ,  $^1\text{H}$  HMQC spectrum of ILV-methyl labeled Pin1WW2 in  $\alpha_7\alpha_7$ , 50°C (blue), with the spectrum of the free Pin1WW2 shown for comparison (green). Pin1WW2 is a stabilized mutant of Pin1WW, Fig. S12a. The melting temperatures for WT Pin1WW and Pin1WW2 are 59°C and 77.5°C, respectively<sup>2</sup>. **b-c**,  $^1\text{H}$   $R_2$  rates for the slowly relaxing methyl proton transitions<sup>3</sup> of free (green) and  $\alpha_7\alpha_7$  (blue) encapsulated Pin1WW2 50°C, 600 MHz (quantified from the peaks corresponding to the folded state). Representative experimental decay curves (circles) from which  $^1\text{H}$   $R_2$  rates for the Ile28 $\delta$ 1 methyl group are extracted based on fits to an exponential (solid curve) are shown in **(b)** along with  $^1\text{H}$   $R_2$  rates for all I,L,V methyl groups of Pin1WW2 in **(c)**. By comparison,  $R_2$  rates have been measured for Pin1WW- $\alpha_7\alpha_7$  and EnHD- $\alpha_7\alpha_7$  (50°C, 600 and 800 MHz, only the unfolded states are observed for these substrates) that are much larger than the

corresponding values for the folded state of the encapsulated Pin1WW2 (**d**). This is to be expected since, unlike the folded domain of the encapsulated Pin1WW2, both Pin1WW and EnHD interact with the walls of the cavity at 50°C. The dependence of  $^1\text{H}$   $R_2$  on field strength for some residues indicates that millisecond exchange processes contribute to relaxation. **e-f**, Distribution of  $^1\text{H}$   $R_2$  rates in  $\alpha_7\alpha_7$  for Ile $\delta$ 1 (**e**) and Leu, Val (**f**) methyl groups measured at 50°C and at a field strength of 600 MHz (grey bars). The distribution of  $R_2$  rates for free Pin1WW is also shown at 50°C, 600 MHz (green bars). Black arrows designate  $^1\text{H}$   $R_2$  rates measured for I,L,V methyl groups of encapsulated EnHD, 50°C (values shown in **d**). Note that for EnHD in  $\alpha_7\alpha_7$  the unfolded state peaks are overlapped and cannot be reliably decomposed. Therefore intensities were measured by numerically summing over each peak cluster and reported relaxation rates are qualitative. Only one of each of Ile, Leu and Val is present in Pin1WW and Pin1WW2 so that this is never a problem for these proteins.

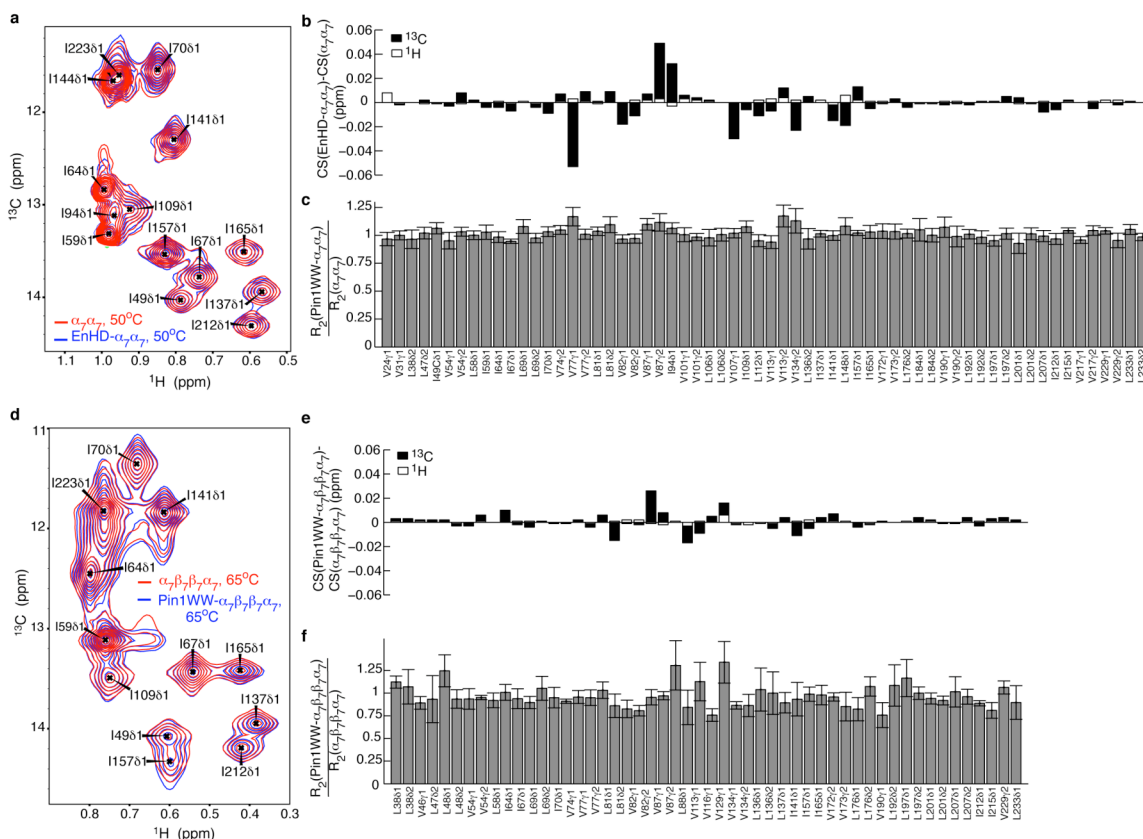


**Figure S10 | The chemical shifts and transverse relaxation rates of  $\alpha$  methyl groups change little upon encapsulation of protonated substrate in  $\alpha_7\alpha_7$  or  $\alpha_7\beta_7\beta_7\alpha_7$ .**

**a-c,** Effect of encapsulating EnHD in  $\alpha_7\alpha_7$ . **a,** Representative region of the  $^{13}\text{C}, ^1\text{H}$  HMQC spectrum of ILV methyl labeled  $\alpha$  in  $\alpha_7\alpha_7$  with (blue) and without (red) encapsulated EnHD, 50°C. **b,** Quantitation of changes in carbon (black) and proton (white) chemical shifts upon encapsulation of EnHD for all peaks in the spectrum. **c,** Ratio of the  $^1\text{H}$   $R_2$  rates for the slowly relaxing methyl proton transitions<sup>3</sup> of  $\alpha$  in  $\alpha_7\alpha_7$ -EnHD relative to  $\alpha_7\alpha_7$  at 50°C, 600 MHz. Note only non-overlapping peaks were quantified. **d-f,** Effect of encapsulating Pin1WW in  $\alpha_7\beta_7\beta_7\alpha_7$  on  $\alpha$  methyl groups. Parts **(d)**, **(e)**, and **(f)** are analogous to **(a)**, **(b)**, and **(c)**, respectively. Note that fewer peaks could be quantified in spectra recorded of  $\alpha_7\beta_7\beta_7\alpha_7$  relative to  $\alpha_7\alpha_7$  because of the poorer quality of the data obtained for the full proteasome. In both **(b)** and **(e)** the chemical shift

changes are very small establishing that either  $\alpha$  does not change conformation, or that structural changes are minor, upon encapsulation of substrate into  $\alpha_7\alpha_7$  or  $\alpha_7\beta_7\beta_7\alpha_7$ . Moreover, the relaxation properties do not significantly change, indicating that the dynamics are also not affected. It is also worth noting that spectra of  $\alpha_7\alpha_7$  or  $\alpha_7\beta_7\beta_7\alpha_7$  containing cys mutants for tethering substrate (in  $\alpha$ -subunits) or mutations rendering the full length proteasome inactive (in  $\beta$ -subunits) were also very similar to spectra of the wild-type constructs.

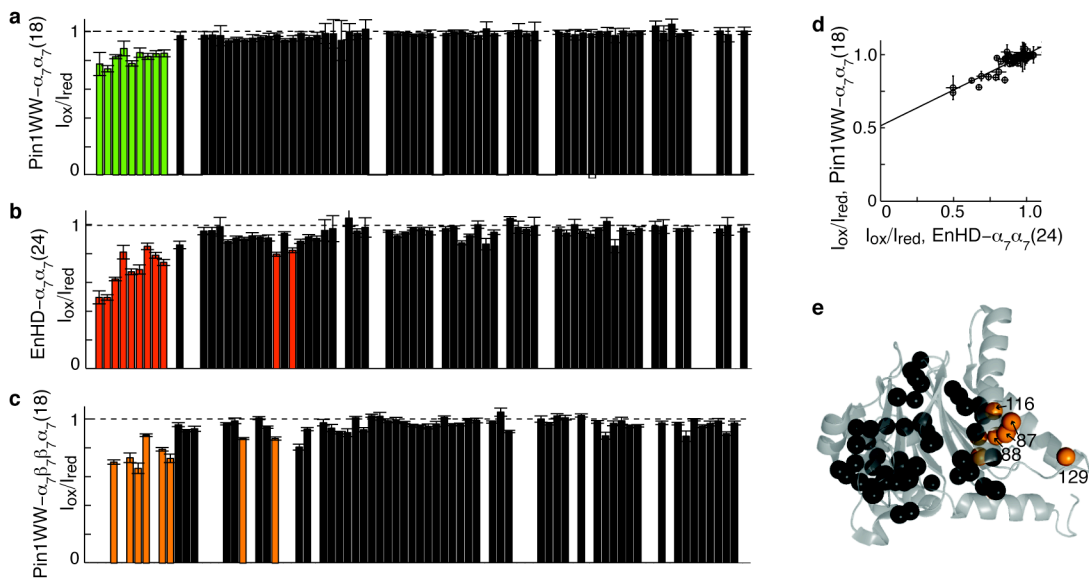


**Figure S11 | Effects of substrate-spin labels on intensities of  $\alpha$  methyl peaks.**

**a-c**, Attenuation of cross-peaks in HMQC spectra recorded on ILV-methyl labeled  $\alpha_7\alpha_7$  ( $50^\circ\text{C}$ ) or  $\alpha_7\beta_7\beta_7\alpha_7$  ( $65^\circ\text{C}$ ) resulting from attachment of a TEMPO nitroxide spin label to residue 18 of Pin1 WW encapsulated in  $\alpha_7\alpha_7$  (**a**), to residue 24 of EnHD in  $\alpha_7\alpha_7$  (**b**) or to residue 18 of Pin1 WW in  $\alpha_7\beta_7\beta_7\alpha_7$  (**c**). Note that the methyl groups are arranged in order of their proximity to the chamber ‘inside’ surface (left to right, groups are located increasingly farther from the surface). Groups with  $>10\%$  decrease in the intensity ratio are colored in green for Pin1WW- $\alpha_7\alpha_7(18)$ , in red for EnHd- $\alpha_7\alpha_7(24)$  and in orange for Pin1WW- $\alpha_7\beta_7\beta_7\alpha_7(18)$ . Shown are intensity ratios obtained by recording spectra either with TEMPO-labeled  $^1\text{H}$  substrate ( $I_{\text{ox}}$ ) or with  $^1\text{H}$  substrate ( $I_{\text{red}}$ ), see below. **d**, Comparison of intensity ratios for TEMPO-labeled EnHD and Pin1WW in  $\alpha_7\alpha_7$ . The pattern of intensity changes for spin-labeled EnHD and Pin1WW are similar (correlation coefficient=0.90) but the extent of attenuation is generally less for Pin1WW), consistent with the spin-label occupying more locations closer to the surface of the cavity when attached to EnHD and suggesting that EnHD interacts more strongly with the surface

than Pin1WW. **e**, Positions with the greatest changes in peak intensities for Pin1WW- $\alpha_7\beta_7\beta_7\alpha_7$ (18) are indicated in the context of the structure of the proteasome antechamber, with changes  $>10\%$  ( $<10\%$ ) shown as orange (black) spheres. The orientation of  $\alpha$  is the same as in Figure 3b. The changes are qualitatively very similar to what was quantified for  $\alpha_7\alpha_7$ , **a**, with methyl residues exhibiting the greatest reduction in intensity upon encapsulation of spin-labeled Pin1WW residing near the inside surface of the  $\alpha$ -ring, just as with  $\alpha_7\alpha_7$ . The slight differences in the PRE profiles reflects the poorer data quality in the case of the full proteasome (absence of peaks or overlap), despite the fact that experiments were performed at  $65^\circ\text{C}$  to offset the increase in molecular weight of the larger particle relative to  $\alpha_7\alpha_7$ . It is noteworthy that intensity changes are only observed for methyl groups located near the inside surface of  $\alpha$ -ring, indicating that it is highly unlikely that Pin1WW leaves the antechamber via the annulus (Figure 1) or dynamic side pores.

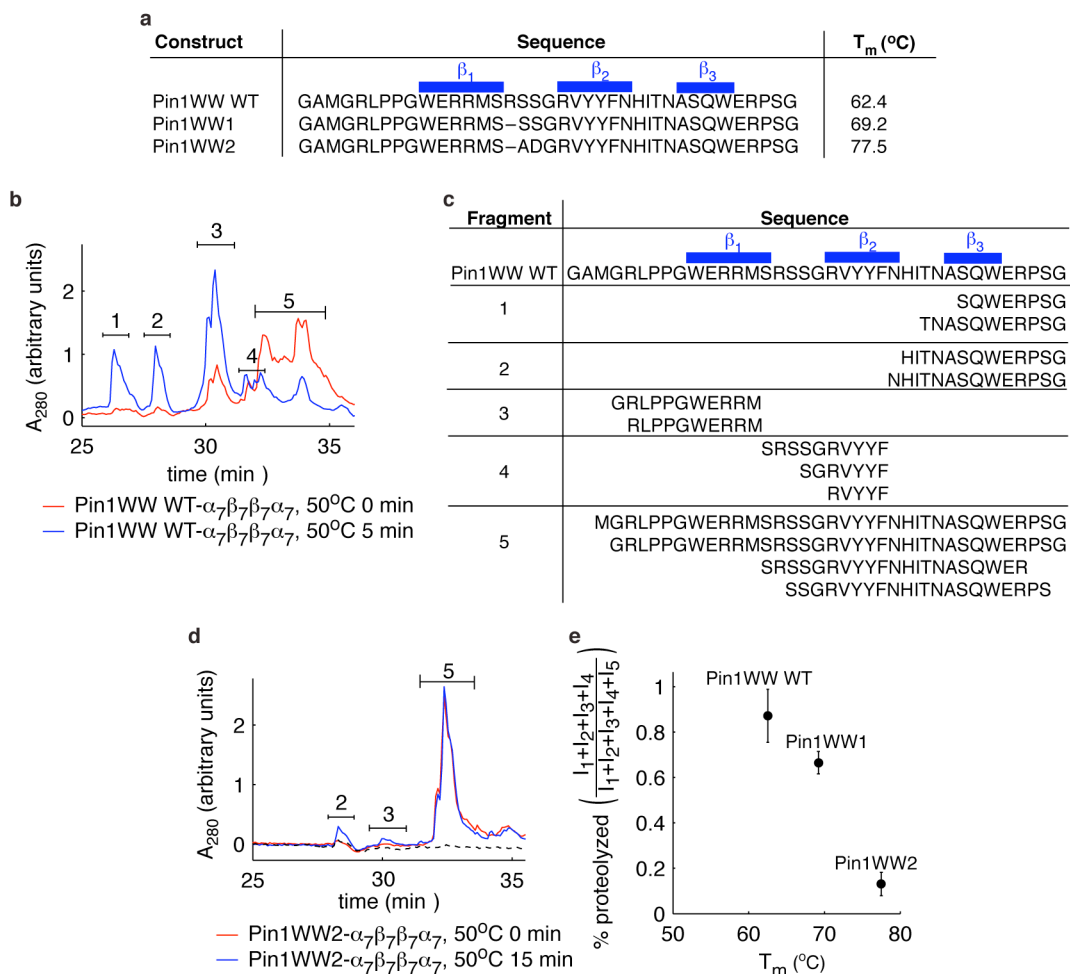


**Figure S12 | Substrate stability correlates inversely with its proteolysis.**

In order to demonstrate that maintaining substrates in an unstructured state inside the antechamber of the proteasome promotes proteolysis, we have measured the hydrolysis of a number of different constructs of the Pin1 WW domain, including WT Pin1WW (referred to as Pin1WW in the text and SI figures) and a pair of stabilized mutants of the Pin1WW domain, Pin1WW1 and Pin1WW2. Proteolysis assays (see below) were carried out using proteasomes that were constructed from  $\alpha$ -subunits containing the S95C mutation and WT  $\beta$ -subunits. Proteasomes, deactivated with the inhibitor Calpain Inhibitor I (4  $\mu$ M proteasome, 5 mM Calpain Inhibitor I,  $K_i \sim 500$  nM (ref 4)), were

loaded with Pin1WW constructs of varying stabilities by cross-linking to the wall of the antechamber at position 95; on average a single substrate was tethered to each antechamber. Loading was achieved by adding 10-fold molar excess substrate over proteasome and incubating at elevated temperature (65°C for Pin1WW WT, 72°C for Pin1WW1, and 80°C for Pin1WW2). Substrate was subsequently released from the tether by first cooling to 5°C (presumably resulting in folding of substrate), and incubating with 0.5 M DTT for 2 hours. Next, to simultaneously activate proteasomes by removing inhibitor and to remove unencapsulated substrate, the reaction was buffer exchanged using a concentrator (MW cutoff = 100 kDa, 5°C). Proteolysis was then allowed to occur by incubation of the substrate- $\alpha_7\beta_7\beta_7\alpha_7$  complex at 50°C for 5 or 15 min. Reactions were quenched upon addition of 6 M Gdn-HCl acidified with 1% TFA, denaturing both proteasome and substrate, and samples were kept frozen until analyzed by reverse phase (RP) HPLC to separate reaction products. Figures **a** and **e** have been repeated from Figure 4 of the main text for clarity.

**a**, Primary sequence of the WW constructs used in this assay, with  $T_m$  values (free form) as indicated<sup>2</sup>. The locations of  $\beta$ -strands are highlighted.

**b,c** RP HPLC elution profiles (monitored at 280 nm) for the Pin1WW WT- $\alpha_7\beta_7\beta_7\alpha_7$  reaction immediately after inhibitor and excess Pin1WW WT was removed (red, 0 min) and after 5 min incubation at 50°C (blue). Note that peaks for proteasome  $\alpha$  and  $\beta$  were also detected but were well resolved from Pin1WW WT (not shown). The content of the 5 major Pin1WW WT peak groups was determined using MALDI mass spectrometry (**c**). A small amount of degradation is observed at the zero time-point (small amount of peak 3, red, and 4 which does not resolve from 5), however very significant levels of degradation are noted after 5 minutes, 50°C (build-up of peaks 1-4, blue). Two

experiments establish that substrate exit and re-entry into different proteasomes does not contribute to the degradation profile at least on a scale of 5 min: (1) After 5 minutes incubation little intact substrate remains. Virtually all of the WW reaction products are outside the proteasome, as assayed by the flow-through from a 100kDa concentrator that retains the proteasome. However, additional incubation (10 more min) at 50°C does not change the degradation profile (data not shown), suggesting that the products do not re-enter the proteasome and undergo further degradation. (2) The observed degradation profile is independent of the concentration of the Pin1WW WT- $\alpha_7\beta_7\beta_7\alpha_7$  complex (data not shown). Note that degradation of encapsulated WW domain is independent of the concentration of Pin1WW WT- $\alpha_7\beta_7\beta_7\alpha_7$ , while proteolysis that proceeds by entrance of substrate that has escaped the proteasome at some earlier stage would be expected to be a function of the concentrations of substrate and  $\alpha_7\beta_7\beta_7\alpha_7$ . The fact that a concentration dependence was not noted establishes that the degradation profiles reflect proteolysis of substrate that remains encapsulated for the duration of the reaction.

**d**, RP HPLC elution profiles (280 nm) for Pin1WW2- $\alpha_7\beta_7\beta_7\alpha_7$  complex immediately after inhibitor and excess Pin1WW2 is removed (red, 0 min) and after 15 min incubation at 50°C (blue). The profile is little changed, establishing that Pin1WW2 does not get degraded over a time-scale that is three-fold longer than for Pin1WW WT where excessive proteolysis has occurred. Pin1WW2 remains inside the proteasome, as it is not present in the flow-through from a 100kDa concentrator used to separate free Pin1WW2 from the proteasome (black, dashed line).

**e**, Correlation between  $T_m$  of the free substrate and extent of substrate proteolysis. Proteolysis of (Pin1WW WT, Pin1WW1, and Pin1WW2) was measured at 50°C after (5 min, 5 min, 15 min) incubation. Note that the extent of proteolysis, as measured by the relative peak areas,  $1+2+3+4 / 1+2+3+4+5$ , does not change for Pin1WW WT and Pin1WW1 between 5 and 15 min (data not shown), reflecting the fact that there are

preferential cleavage sites in the WW domain and that these are already cleaved for Pin1<sup>WW</sup> WT and Pin1<sup>WW1</sup> after 5 min. Substrate  $T_m$  values are decreased upon encapsulation into  $\alpha_7\beta_7\beta_7\alpha_7$  with all three substrates having different relative populations of unfolded / folded states, as established by NMR studies (50°C) described in the text. The inverse correlation between substrate stability and extent of proteolysis implies that the proteasome processes unfolded substrate more efficiently than folded substrates due to either an increased rate of translocation into the catalytic chamber and/or an increase in the chemical step of hydrolysis. Our data do not allow us to distinguish between these possibilities.

Peak	% Folded	
	$\alpha_7\beta_7\beta_7\alpha_7$	$\alpha_7\alpha_7$
I28 $\delta$ 1	29.9 $\pm$ 4.9	30.2 $\pm$ 3.8
V22 $\gamma$ 1	32.1 $\pm$ 8.3	31.8 $\pm$ 4.5
V22 $\gamma$ 2	23.3 $\pm$ 9.5	27.1 $\pm$ 10.3
L7 $\delta$ 1	17.8 $\pm$ 10.5	20.8 $\pm$ 4.0
L7 $\delta$ 2	29.9 $\pm$ 9.5	26.2 $\pm$ 3.4

**Table S1 | The populations of the folded state of Pin1WW2 encapsulated in  $\alpha_7\beta_7\beta_7\alpha_7$  and in  $\alpha_7\alpha_7$ , 65°C, are nearly identical.**

Quantitation of the fraction of Pin1WW2 folded at 65°C in  $\alpha_7\beta_7\beta_7\alpha_7$  and  $\alpha_7\alpha_7$ , computed for each labeled methyl group from the peak intensities of the folded and unfolded states (Figure S8). Pin1WW2 is destabilized to a similar extent in  $\alpha_7\beta_7\beta_7\alpha_7$  and  $\alpha_7\alpha_7$ . For reference, free Pin1WW2 is 85% folded under these conditions.

## References

1. Fersht *Structure and Mechanism in Protein Science* (W H Freeman & Co, 1999).
2. Jäger, M., Zhang, Y., Bieschke, J., Nguyen, H., *et al.* Structure-function-folding relationship in a WW domain. *Proc. Natl. Acad. Sci. U S A* **103**, 10648-10653 (2006).
3. Tugarinov, V. & Kay, L. E. Relaxation rates of degenerate 1H transitions in methyl groups of proteins as reporters of side-chain dynamics. *J. Am. Chem. Soc.* **128**, 7299-7308 (2006).

4. Huffman, H. A., Sadeghi, M., Seemuller, E., Baumeister, W. & Dunn, M. F. Proteasome-cytochrome c interactions: a model system for investigation of proteasome host-guest interactions. *Biochemistry* **42**, 8679-8686 (2003).